A smart load-speed sensitive cooling map to have a high- performance thermal management system in an internal combustion engine

Alireza Naderi[a], Ali Qasemian[a], Mohammad Hasan Shojaeefard[b], Saman Samiezadeh[a], Mostafa Younesi[a], Ali Sohani[c], SiamakHoseinzadeh[d],*

[a]Automotive Fluids and Structures Analysis Laboratory, School of Automotive Engineering, Iran University of Science and Technology, Tehran, Iran
[b]Faculty of Mechanical Engineering, Iran University of Science and Technology, Tehran, Iran
[c]Lab of Optimization of Thermal Systems' Installations, Faculty of Mechanical Engineering-Energy Division, K.N. Toosi University of Technology, P.O. Box: 19395-1999, No. 15-19, Pardis St., Mollasadra Ave., Vanak Sq, Tehran, 1999 143344, Iran
[d]Centre for Asset Integrity Management, Department of Mechanical and Aeronautical Engineering, University of Pretoria, Pretoria, South Africa

*Corresponding author.

hoseinzadeh.siamak@gmail.com
Hosseinzadeh.siamak@up.ac.za

Highlights

- The coolant flow rate is 10.6% lower than the conventional system in the full load.
- 21.3% changes in comparison to the conventional cooling is seen for the part load.
- More uniform temperature distribution is achieved by applying smart cooling.
- Neither overcooling in the part load nor undercooling in the full load happens.
- Compared to the conventional cooling, pump power consumption gets 44.3% lower.

Abstract

Considering the fact that electrification is increasingly used in internal combustion engines, this paper aims at presenting a smart speed-load sensitive cooling map for better thermal management. For this purpose, first, thermal boundary conditions for the engine cooling passage were obtained by thermodynamic and combustion simulation. Next, the temperature distribution of the cooling passage walls was determined using conjugate heat transfer method. Then, the effect of engine load on wall temperature distribution was investigated, and it was observed that in the conventional mode where the cooling flow is only affected by the engine speed, the engine is faced with over-cooling and under-cooling. Therefore, the optimum flow for cooling the engine was achieved in such a way that the engine is hot enough and kept free from damage, while the engine has a more uniform temperature distribution. These calculations were performed by considering the boiling phenomenon. The results showed using the cooling map leads to a significant reduction in coolant flow, which in turn reduces the power consumption of the water pump and size of the radiator. Moreover, fuel consumption, hydrocarbon emission production, and the needed power of the coolant pump are enhanced by 2.1, 8.6, and 44.3%, respectively.

Keywords: Cooling map; Electrification; Power consumption reduction; Internal combustion engine;

Nomenclature

Nomenclature

A	Area (m^2)
q''	Heat flux ($\frac{W}{m^2}$)
h	Heat transfer coefficient ($\frac{W}{m^2.K}$)
v	Velocity ($\frac{m}{s}$)
P	Pressure (kPa)
$\dot{m}$	Mass flow ($\frac{kg}{s}$)
r_c	Compression ratio
C_p	Specific heat coefficient ($\frac{J}{kg.K}$)
T	Temperature (K)
t	Time (s)
u	Velocity ($\frac{m}{s}$)
k	Heat conductivity ($\frac{W}{m.K}$)
Re	Reynolds
D	Diameter (m)
Pr	Parental
S	Suppression factor
h_{nb}	Nucleate boiling convection heat transfer coefficient ($\frac{W}{m^2.K}$)
T_{sat}	Saturation temperature (K)
k_c	Coolant conductivity ($\frac{W}{m.K}$)

Abbreviations

HTC	Heat transfer coefficient
I.C	Internal combustion
TC	Turbocharger
PIV	Particle image velocimetry
SI	Spark ignition
RPM	Round per minute
BC	Boundary condition
1D	One dimensional
3D	Three dimensional
CHT	Conjugated heat transfer
CFD	Computational fluid dynamics
ROHR	Rate of heat release
HCCI	Homogeneous charge compression ignition
CFR	Cooperative fuel research
FEM	Finite element method
THC	Total hydrocarbon
NOx	Nitrogen oxides
CO	Carbon monoxide
GDI	Gasoline direct injection
CO_2	Carbon dioxide
WOT	Wide open throttle

Greek symbols

ρ	Density ($\frac{kg}{m^3}$)
$\varnothing$	Dissipation
μ	Viscosity ($\frac{kg}{m.s}$)
θ	Throttle angle (degree)

1. Introduction

Engine cooling is an important area in the design of the internal combustion (I.C) engines [[1], [2], [3], [4]], because it has a direct influence on the efficiency [5,6], fuel consumption [7,8], and emissions of the system [[9], [10], [11]].

The use of a mechanical pump in the conventional cooling system decreases engine efficiency due to excessive cooling during cold-start or part-load conditions [12]. Moreover, when the engine rotational speed is high, the excessive flow of cooling fluid can reduce combustion efficiency [13,14]. Moreover, since the cooling pump is often working even when it is not needed, the fuel consumption increases, as well [15].

In the conventional cooling system, a mechanical pump is linked to the crankshaft, and consequently, the coolant flow rate does not reach the required level during low-speed and high load operation (e.g., driving uphill) [[16], [17], [18]]. As a result, the engine temperature rises excessively. Similarly, while driving downhill on a steep, due to the high engine speed, excessive coolant flow is circulated, which results in lower thermal efficiency [[19], [20], [21]].

Considering the mentioned points, the need for the use of innovative engine cooling systems has increased over the years, which leads to the development of different technologies such as intelligent cooling systems, precision cooling systems, nucleate boiling cooling systems, and so on. Among the variety of developed technologies, electric cooling pumps are a good case in point.

Electric pumps becoming increasingly popular with the advancement of the electronics industry can be controlled by the engine control unit regardless of engine speed. It can bring benefits to engine performance, such as improving the engine warm-up condition [22], which can reduce fuel consumption and emissions during cold-start [23]. Moreover, the size of the cooling system

becomes smaller, which is taken into account as another advantage of the electric pumps compared to the mechanical ones. For instance, as it was shown in the study of Cho et al. [24], by using electric pumps, the radiator size for the investigated engine can be reduced by 27% of the original size. It is worth mentioning that the improvement refers to the enhancement in fuel consumption, hydrocarbon emission production, and the needed power of the coolant pump.

1.1. Literature review

In order to discuss the novelty of the study, the literature review is divided into two parts. One part investigates the studies done with the subject of bringing new cooling systems. Another part provides an overview of the works carried out in the engine thermal modeling area. As it will be described in detail, in order to study the performance of a cooling system, thermal modeling of the engine is necessary.

1.1.1. The studies with the subject of bringing new cooling systems

Choi et al. [25], Jeong et al. [26], and Wang et al. [27] investigated the effect of a new cooling system on the exhaust emissions and fuel consumption of diesel engines experimentally. They used a clutch-type water pump, variable speed electric pump, and variable speed electric radiator fan in the cooling system to control coolant flow rate and temperature. The results of these studies showed that using electrical actuators instead of mechanical ones, the engine performance was improved from different points of view. For instance, based on the results of the study conducted by Jeong et al. [26], CO_2 emission was reduced by around 3%, while Wang et al. [27] demonstrated that the fuel economy was improved 3%–5%.

As another study in the field, Wagner et al. [28] investigated the enhancement in the performance of an engine when a smart thermostat valve and a variable speed pump were used in a diesel engine cooling system. They employed numerical simulation to study the thermal behavior of the engine and determined required heat rejection per unit volumetric flow rate of the pump.

Moreover, Negandhi et al. [29] carried out an extensive study investigating the use of dual-mode coolant pump (DMCP) in the cooling system of a V6 diesel engine. They used GT-SUITE software to control coolant temperature with the pump speed. It was demonstrated that the fuel economy was improved by more than 2% by replacing DMCP with the conventional mechanical pump.

The experimental works done by Cai et al. [30], Chastain et al. [31], Shin et al. [32], and Mohamed et al. [33,34] have focused on developing intelligent cooling systems for SI engines. In the mentioned investigations, innovative cooling strategies, such as electromagnetic clutch water pumps and variable position electromagnetic thermostat (VPEMT), were used for modification of SI engine cooling system. Like what has been found for diesel engines, the improvement in the system performance has been shown for SI engines. For example, the results of the study performed by Mohamed et al. [34] indicated that, after applying the proposed advanced coolant control strategy, the warm-up period could be decreased by 31% compared to the conventional system. In addition, employing the intelligent engine cooling method employed in the study of Cai et al. [30] was accompanied by 7% decrease in the fuel economy.

Haghighat et al. [35] also developed an experimental model for a proposed dual-fuel engine cooling system, which worked based on the engine speed. The developed model was employed to evaluate the improvement in engine performance. It was found that by replacing the proposed

engine intelligent cooling system with the conventional one, the HC and CO emissions decreased by 5.3% and 6.1%, respectively, while fuel consumption had 1.1% reduction during NEDC cycle operation. Castiglione et al. [36] also conducted experiments to study nucleate boiling in small displacement spark S.I engine. Several parameters, such as temperature and pressure of coolant as well as wall temperature, were measured.

1.1.2. The works carried out in the engine thermal modeling area

In addition to proposing a smart cooling system and evaluating the performance improvement of that, studying the thermal behavior of the engine is taken into account as another hot topic in the field of intelligent cooling. In such investigations, the criteria such as temperature field and heat flux have been investigated by experimental analysis or numerical methods, including CFD, FEM, CHT, 1D, and quasi dimensional simulations in some studies, as reviewed in the following.

As an example of the studies with the subject of studying the thermal behavior, Annabatulla et al. [37] used STAR-CCM+ and design of experiment (DOE) to improve the engine design coolant passage. Having developed the approach, thermal behavior was also analyzed. In another study, Mohamed Hassan et al. [38] applied STAR-CD to demonstrate the consequences of water injection on the wall heat transfer and temperature. Moreover, in order to simulate engine heat transfer after shut down considering nucleate boiling, Ali et al. [39] studied the combination of integrated heat transfer analysis and CFD finite volume method with a triangular grid.

Decan et al. [40,41] also took advantage of using open-source software, Open FOAM®, to carry out simulations of a CFR engine, under both motored and HCCI operation, with special attention on the performance of various heat flux models. Modeling included the equilibrium wall models as in the standard use, an improved empirical heat flux correlation, and a numerically intensive low Reynolds formulation. Moreover, for analyzing the heat flux distribution on the walls of a hydrogen-air mixture cylinder during the compression stroke, Schmitt et al. [42] used direct numerical simulation (DNS) and investigated the relationship between the temperature field and the local heat flux distribution.

In order to explore the accuracy of the single zone thermodynamic model compared to the 3D CFD model, Mauro et al. [43] carried out a comparative study. Considering the simplicity and speed of the single-zone model, they illustrated that the estimation of the heat release was reasonably accurate, which means the results of that can be the basis of the combustion process. Furthermore, Jo et al. [44] studied the thermal efficiency of a downsized turbocharged engine with respect to the rate of compression, considering the knock limitation by 1D quasi dimensional simulation.

The effectiveness of wall temperature on evaporation and mixing characteristics of impingement spray was also examined by Wu et al. [45]. They investigated the combustion process and emissions of GDI engines as well. In addition, they provided an integrated approach to accurately estimate the in-cylinder combustion process and engine temperature field consisting of engine head/block/gasket and water jacket elements. In this research, like the last two reviewed papers, the 1D simulation was applied to find boundary conditions of transient pressure and temperature and gas side time-averaged HTC.

Saric et al. [46] and Berni et al. [47] worked on the role of the law of the wall in the reliability of heat transfer parameters of an SI engine through the wall. Saric et al. [46] found that the standard or low-Re variants of the k-ε turbulence model were not appropriate for this purpose.

Considering this point, they suggested the compressible wall function of Han and Reitz in the framework of hybrid wall treatment by the k-ζ-f turbulence model as a more reliable option.

Furthermore, Berni et al. [47] proposed a novel heat transfer model to simulate wall heat fluxes, which was in good agreement with both the experimental engine thermal survey and local temperature measurements for all engines and operating conditions. In that study, CHT and 3D-CFD methods were used to investigate the thermal behavior of the engine. The simulation results were compared with Han and Reitz's and Angelberger's models [48,49]. These two models are both known and they are available in CFD commercial codes, and operate properly in engine test case (i.e., the GM pancake).

With respect to 3D-CFD and CHT method, Cicalese et al. [50] used this method in a high power-density diesel engine and indicated the predictive capabilities of this technique both for global thermal balance and local engine temperature distribution.

Broatch et al. [51] focused on the heat transfer of the walls in a spark ignition (SI) engine. In this study, in order to reduce the required computing time for performing CHT simulation, the authors replaced the combustion process with the Rate of Heat Release (RoHR) derived from a CFD calculation. They proved that the CHT-RoHR approach provides an acceptable outcome in regards to spatially averaged values throughout the whole engine cycle while it is able to reduce the computational cost significantly.

Moreover, Arada et al. [52] simulated the velocity distribution and wall heat flux near the engine wall. With highly resolved calculation mesh, they were able to change the turbulent Reynolds number wall in the boundary layer according to the near-wall flow condition. Based on the obtained result, a new model was formulated by which the prediction accuracy of wall heat flux even in near-wall flow was improved, especially in HCCI engines.

Ma et al. [53] verified the validity of the equilibrium and non-equilibrium wall-function model in predicting wall heat transfer of internal combustion engines. Verification of the validity was done by simultaneous high-speed, high-resolution particle image velocimetry and heat-flux measurements. According to the results, it was found that the equilibrium wall-function model under predicts the heat flux significantly. Nonetheless, the non-equilibrium wall model was shown to be able to capture the structure and dynamics of both momentum and thermal boundary layers adequately.

Li and Kong [54] established a numerical procedure, coupling in-cylinder combustion modeling with CHT, to model in-cylinder flow and solid heat conduction at the same time. In this research, in both the fluid and solid domains, the temperature fields were coupled by applying equal heat flux and equal temperature at the fluid–solid interface. The results showed a correct prediction of unsteady and non-uniform temperature distributions on the chamber surface.

Zhang [55] applied CHT into KIVA-4 in order to investigate solid engine components' temperature range. Based on the results, the CHT modeling provided a reasonable, realistic temperature distribution on the chamber wall compared to the constant wall temperature. In addition, Keum et al. [56] suggested and simulated a modified wall function model by KIVA-3, in which the effect of variable density and variable viscosity was taken into account.

1.2. Gap of the study

According to what discussed, to the best of our knowledge, the following item is taken into account as the gap of the research:

- The intelligent cooling strategies to utilize the electric pump, including the reviewed ones, are introduced in a way that only the speed has been taken into account. It means that, the load, as a very important effective parameter, has not been considered to obtain the performance map for cooling the engine. As discussed in detail in the results and discussion section of this study, not considering the load leads to overcooling and undercooling of the engine which is known as a harmful phenomenon in the internal combustion engines.

1.3. Novelty of the research

Based on the gap of the study, which has been mentioned in the previous part, to contribute to this line of research, this study takes the initiative in determining the required coolant flow rate of a downsized turbocharged I.C engine as a function of load and speed based on the interaction of 1D and 3D simulations. It is to be noted that, as the comprehensive literature review demonstrates, to the best of our knowledge, none of the previous studies has developed such a cooling system that is affected by both engine load and speed simultaneously. Accordingly, this study aims at proposing a scientific and engineering methodology, with the least computational complexity, based on 1D and 3D simulations in order to obtain the required flow rate of the cooling system as a function of engine load and speed. In this method, instead of full CHT, temperature and heat transfer coefficient is calculated by 1D simulation and then, as boundary conditions, inserted into a 3D CFD simulation. Applying 1D simulation leads to a significant decrease in computing volume and run-time. Moreover, as it has been already discussed in the literature review part, the employed methodology is accurate to describe the system performance. This concept is introduced as a "smart speed-load sensitive engine cooling map" in the present study. By providing the developed performance map, an appropriate solution to employ the water pump efficiently is introduced.

1.4. Structure of paper

This research is organized as follows. After this part (introduction), the methodology is explained. Then, the results are presented, and discussion on them was done. Finally, the main outcomes of the study were given in the conclusion part.

2. Methodology

The proposed methodology to determine the smart speed-load sensitive engine cooling map is introduced in this section. All the required information, including the description about 1D and 3D simulations and validation, in addition to the details about modeling the boiling are explained. Moreover, the specifications of the investigated I.C engine are also given.

Fig. 1 shows the flowchart of the methodology applied in this study. As it is shown, the presented methodology obtains the suitable coolant mass flow rate based on the following procedure:

1. Initially, the 1D simulation for the engine is carried out.

2. Then, the pressure, temperature, and HTC are determined in different values for load and speed.
3. After that, the BCs, including mean temperature, heat transfer, and so on, are derived.
4. Next, 3D simulation is done by employing CHT.
5. Here, setting the mass flow rate is done. As the first guess, the value for the conventional cooling system can be used.
6. After that, the temperature distribution is found.
7. Then, the effect of boiling is considered using the developed MATLAB code.
8. The values of temperature for the critical regions are checked:

- If it is equal to the appropriate set-point, the required mass flow rate is introduced as the map suggested one.
- Otherwise, the mass flow rate changes one step. If with the current value, over cooling happens, the new value decreases one step. On the other hand, if under cooling takes places, the new value increases one step, and then, the process is repeated from stage 5.

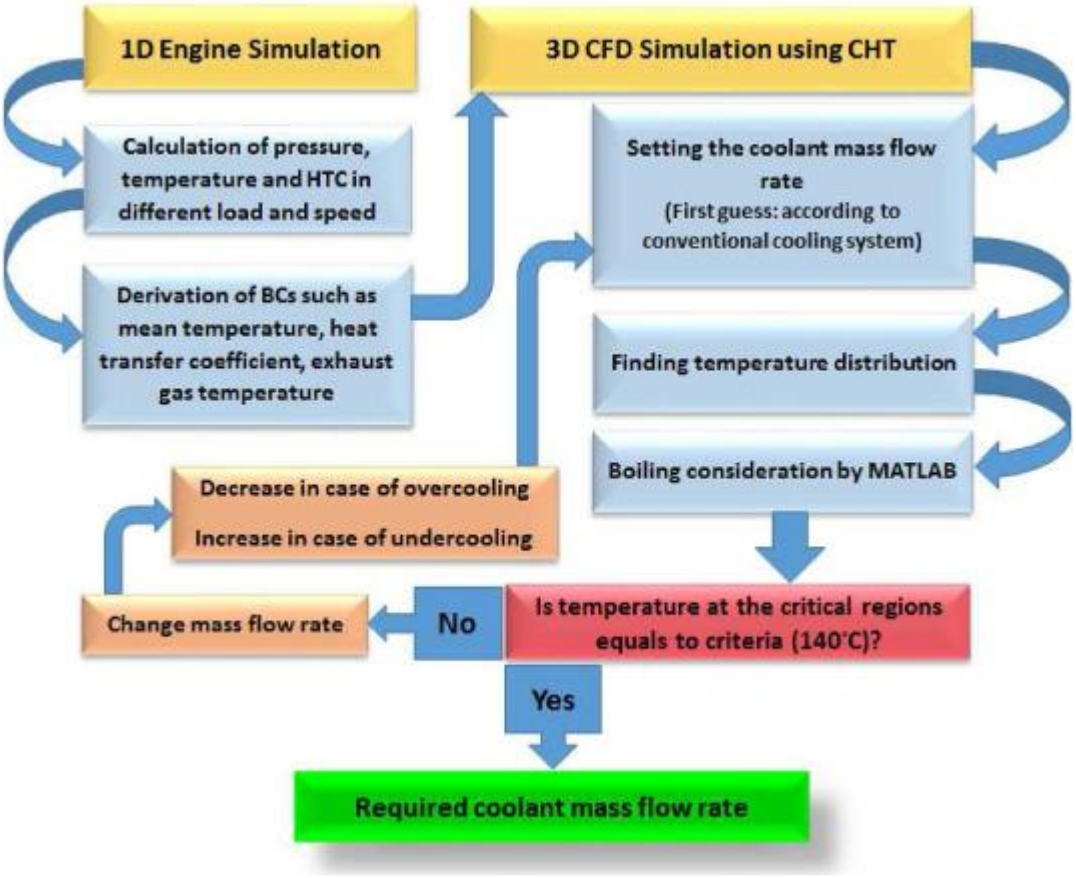

Fig. 1. Flowchart of the methodology used in the present study.

2.1. The investigated internal combustion engine

Today, the need for energy sources with high energy density has made the use of technologies such as downsizing and turbocharging a necessity. Energy management and cooling of this kind of high energy density engines should be carefully considered and studied. As a result, this study investigates a downsized turbocharged internal combustion engine. The specifications of the investigated engine are given in Table 1.

Table 1. The specifications of the investigated engine.

Engine characteristics	
Type	SI
Charging	TC
Injection type	Port fuel infection (PFI)
No. of cylinder	4
Volume	1649 cc
Bore	78.6 mm
Stroke	85 mm
Valves	4 per cylinder
Compression ratio	11.2
Maximum torque	215 Nm at 4800 rpm
Maximum power	150 hp at 5500 rpm

2.2. 1D simulation

In order to determine boundary conditions (BCs) of combustion chamber, GT-POWER software is used. These parameters are used as BCs in 3D simulations. Processes such as combustion, fuel injection, intake, and exhaust gas flow are modeled 1D.

As various engine operating conditions, five different engine speeds 1500, 2500, 3500, 4500 and 5500 rpm at four different throttle angles including 35°, 45°, 67° and 90° are chosen in this study. Therefore, twenty different cases are considered for investigating the effects of engine load and speed on the coolant flow rate. In Table 2, the corresponding brake mean effective pressure (BMEP) of the engine at the mentioned conditions for the throttle position (THPS) are given in two engine speeds of 3500 and 5500 rpm.

Table 2. Engine BMEP at different throttle position and two engine speeds.

5500 rpm		3500 rpm	
THPS (degrees)	BMEP (bar)	THPS (degrees)	BMEP (bar)
90	18.00	90	18.00
67	14.25	67	15.21
45	9.90	45	10.20
35	8.00	35	8.00

Following this, in each given speed and throttle angle, in-cylinder temperature and heat transfer coefficient (HTC) is calculated. Then, equations (1), (2)) are used to obtain the average HTC and temperature as BCs [57].

$$\overline{h}_g = \frac{1}{4\pi} \int_0^{4\pi} h_g \, d\theta \tag{1}$$

$$\overline{T}_g = \frac{1}{4\pi \overline{h}_g} \int_0^{4\pi} h_g T_g \, d\theta \tag{2}$$

The heat flux into the containing walls changes continuously from a small negative value during the intake process to a positive value of order several megawatts per square meter early in the expansion process. Some studies focused on the effect of in-cylinder pressure and temperature oscillation on the wall temperature of the internal combustion engine [58,59]. However, Heywood [60] put, investigators have concluded that the assumption of quasi-steady heat transfer is sufficiently accurate for most calculation purposes.

The concept of penetration depth is highly considerable here. The penetration distance δ is a measure of how far into the material fluctuations about the mean heat flux penetrates. As mentioned by Ferguson [57], for distances x greater than , the temperature profile is more or less steady and driven only by the time-average heat flux. Since the length δ is small compared with the dimensions (wall thickness, bore, etc.) over which conduction heat transfer occurs, the conduction heat transfer in the various parts can be assumed steady and driven by the average flux.

Here the oscillating flux applied to the cylinder acts as the oscillating force on the crankshaft. Just as there is no fluctuation at the engine outlet shaft due to the flywheel, there is no temperature fluctuation in the coolant side of cylinder head water jacket due to the metal thickness. The most important reason for this phenomenon is related to the high speed of engine cycles.

One of the boundary conditions needed for 1D simulation is the wall temperature of the different parts of the combustion chamber. After examining the small effect of the wall temperature on the gas temperature and the heat transfer coefficient, the average temperature of each part is set as given in Table 3 using three-dimensional simulations and data provided by the manufacturer and validated references [57,60].

Table 3. The combustion chamber wall temperature as the boundary condition of 1D simulation.

Engine part	Wall temperature (°C)
Cylinder block	145
Cylinder head	195
Piston	285

2.3. 3D modeling and meshing

Pro-Engineer software is used for 3D CAD modeling of the engine. In this software, the engine is discretized into three main parts: cylinder block, cylinder head, and coolant passage with all details.

Cylinder block, head, and coolant passage are meshed in HYPERMESH. High accuracy in complex areas and areas with rough angles are the most important advantage of this software. Parts of the coolant passage, cylinder block, and cylinder head mesh are depicted in Fig. 2, Fig. 3, and Fig. 4, respectively.

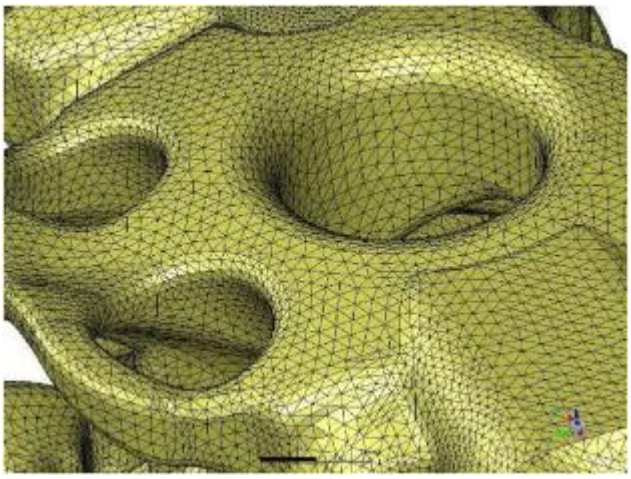

Fig. 2. Mesh of coolant passage in HYPERMESH.

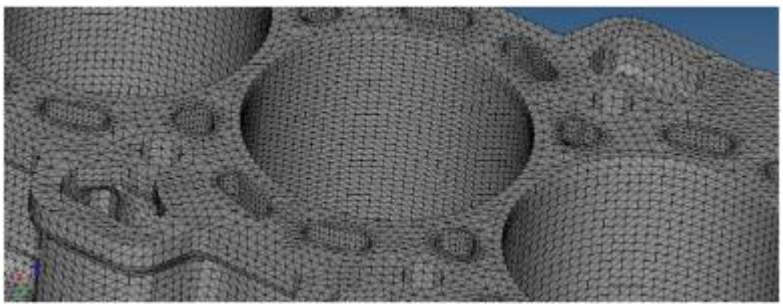

Fig. 3. Mesh of cylinder block in HYPERMESH.

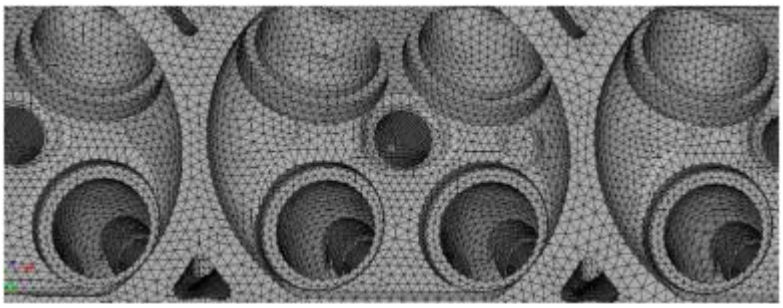

Fig. 4. Mesh of cylinder head in HYPERMESH.

In order to achieve an accurate and stable solution, tetra – hexagonal elements are utilized for mesh generating. Fig. 5 illustrates total mesh quality by skewness and aspect ratio. According to fluent guide [61], a precise mesh should have skewness lower than 2 and aspect ratio lower than 5. Furthermore, this mesh should be small enough near sensitive areas.

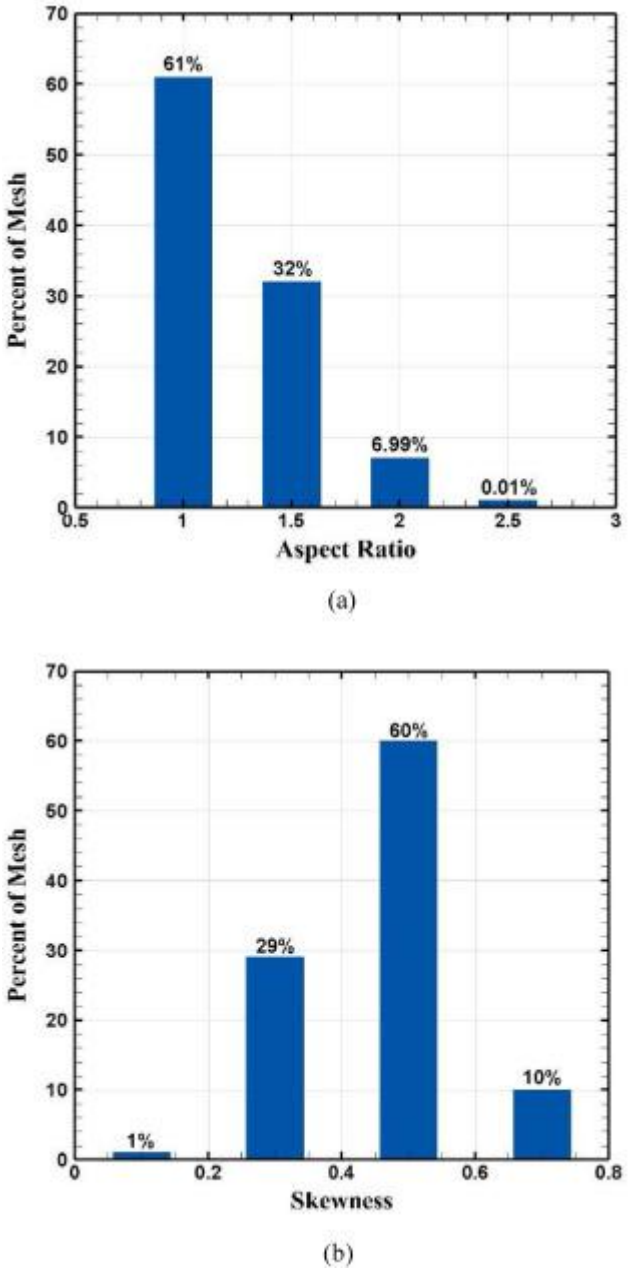

Fig. 5. Mesh quality in HYPERMESH. (a) Aspect ratio, (b) Skewness.

According to Fig. 5, the total percentage related to elements that have an aspect ratio lower than 2 is 93%, and a negligible amount of them have an aspect ratio greater than 3 (0.01%). Moreover, up to 90% of the elements have a skewness lower than 0.5. As demonstrated in Fig. 6, mesh size near sensitive areas such as the exhaust ports are smaller and finer than other areas. The minimum and maximum mesh sizes are 0.15 mm and 4.4 mm, respectively. Total elements used in this model are 7,178,833 which include 2,832,881 elements for coolant passage, 2,804,450 elements for cylinder head and 1,541,522 elements for cylinder block.

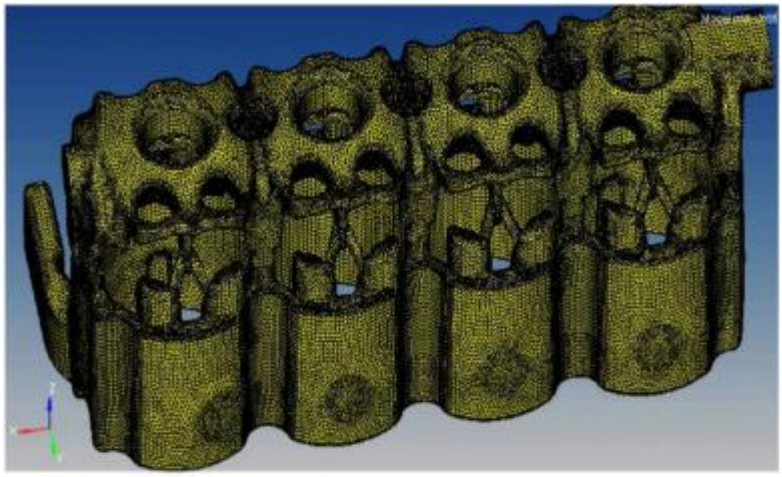

(a)

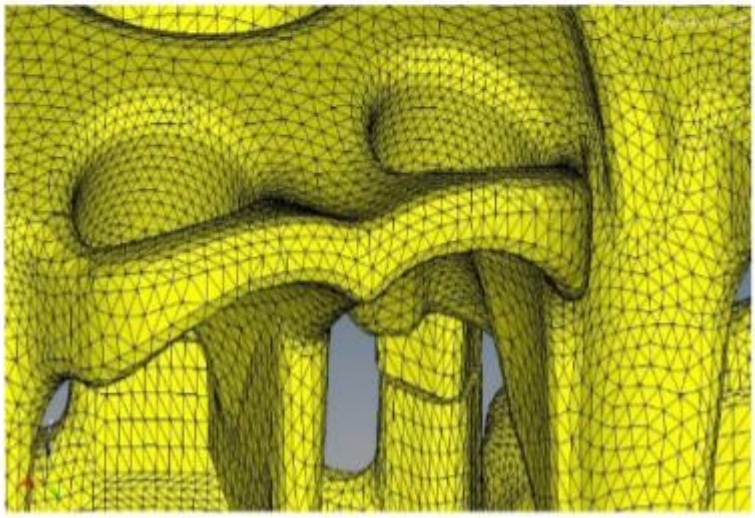

(b)

Fig. 6. Mesh size in different area in HYPREMESH. (a) Total coolant mesh. (b) Different mesh size.

2.3.1. Governing equations

Equations (3)–(5) are three main equations of fluid flow; continuity, momentum, and energy [62].

$$\frac{\partial \rho}{\partial t} + \frac{\partial}{\partial x_i}(\rho u_i) = 0 \tag{3}$$

$$\frac{\partial}{\partial t}(\rho u_i) + \frac{\partial}{\partial x_j}(\rho u_i u_j) = -\frac{\partial P}{\partial x_i} + \frac{\partial \tau_{ij}}{\partial x_i} + \rho g_i + F_i \tag{4a}$$

$$\tau_{ij} = \left[\mu\left(\frac{\partial u_i}{\partial x_j} + \frac{\partial u_j}{\partial x_i}\right)\right] - \frac{2}{3}\mu\frac{\partial u_l}{\partial x_l}\delta_{ij} \tag{4b}$$

$$\rho\frac{Dh}{Dt} - \nabla.k\nabla T - \nabla.\left[\sum_j \gamma_j h_j \nabla m_j\right] - \mu\emptyset - \frac{DP}{Dt} - S = 0 \tag{5a}$$

$$\emptyset = \left[\frac{\partial u_i}{\partial x_j} + \frac{\partial u_j}{\partial x_i} - \frac{2}{3}\mu\frac{\partial u_l}{\partial x_l}\delta_{ij}\right]\frac{\partial u_j}{\partial x_i} \tag{5b}$$

2.3.2. Solution method

CHT method is used for 3D simulation of the engine in FLUENT software. In regard to turbulence modeling, k-ϵ solution method is chosen due to shorter run-time with the same accuracy in comparison with other turbulence models. The “standard wall function” is used for fluid flow near the walls.

is higher than 100 in all regions [61].

2.3.3. Boundary conditions

A mixture of 50-50 water and ethylene glycol is considered as engine coolant with thermo-physical properties given in Table 4.

Table 4. Coolant properties at 100° C

property	symbols	units	quantity
density	ρ	$\frac{kg}{m^3}$	1055
Specific heat	C_p	$\frac{J}{kg.K}$	3730
Heat conductivity	k	$\frac{W}{m.K}$	0.415
viscosity	μ	$\frac{kg}{m.s}$	0.00095

Convective heat transfer coefficient at WOT and part load, the temperature of the combustion chamber, and also exhaust port temperature obtained by 1D simulation in different engine speeds and WOT are shown in Fig. 7, Fig. 8, Fig. 9, Fig. 10, respectively

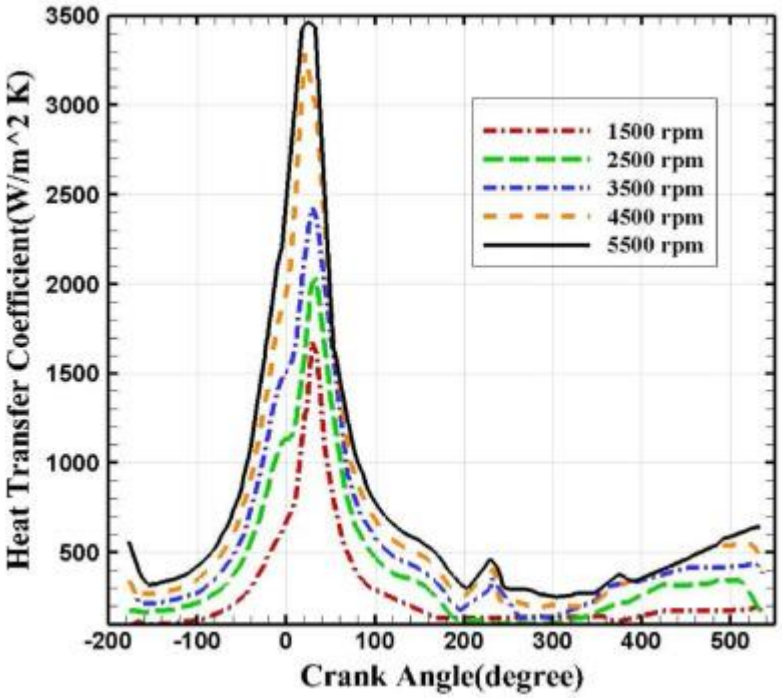

Fig. 7. Combustion chamber HTC in different engine speeds and WOT.

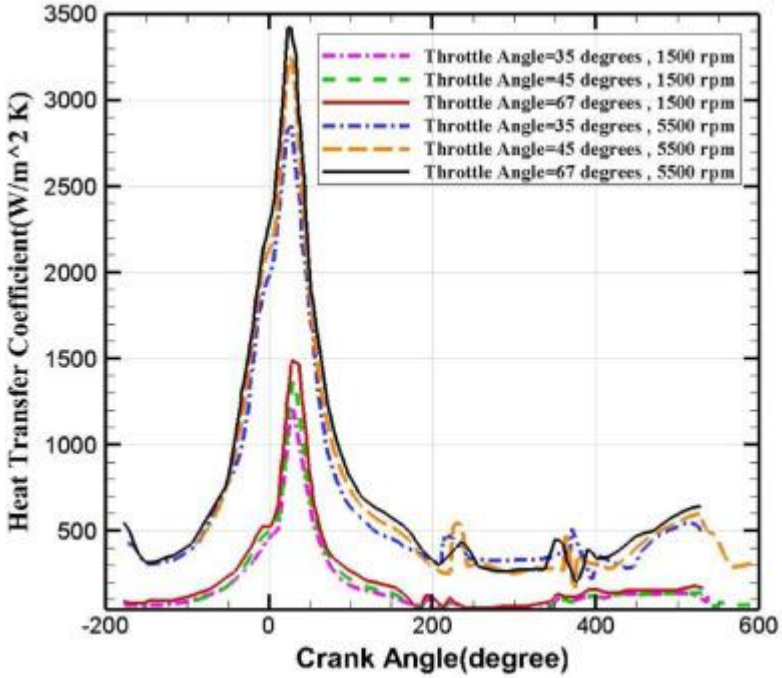

Fig. 8. Combustion chamber HTC in different loads and engine speed.

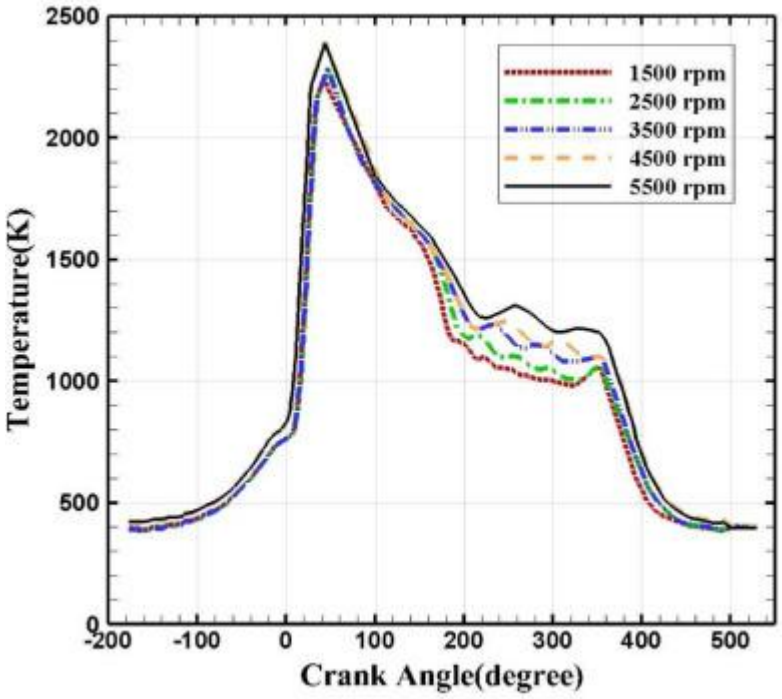

Fig. 9. Combustion chamber temperature in different engine speeds and WOT.

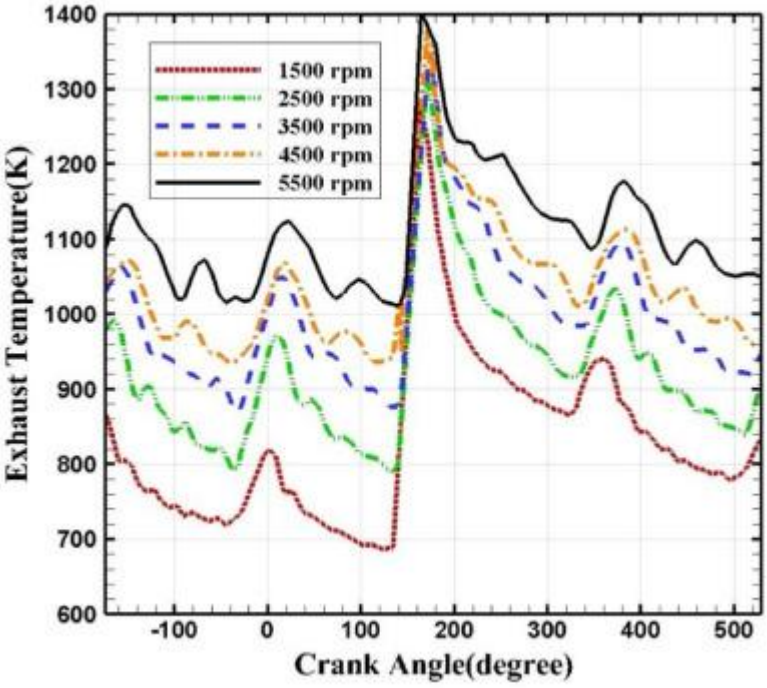

Fig. 10. Exhaust port temperature in different engine speeds and WOT.

HTC of exhaust and intake ports, in which one-dimensional simulation cannot be sufficient, some correlations such as equation (6) is applied, respectively [63].

$$h = \frac{k}{d} 0.07 \overline{Re}^{3/4} \tag{6}$$

It should be noted that the values of HTC and temperature of under hood are given in the [49,64]. Furthermore, in FLUENT software, velocity inlet boundary condition is used for defining coolant flow properties at inlet boundary, and pressure outlet boundary condition is considered for specifying pressure of coolant flow at outlet boundary. Table 5 gives the information related to the coolant mass flow rate of the engine measured experimentally.

Table 5. Coolant mass flow rate in different engine speeds.

Engine speed (rpm)	Coolant mass flow rate (kg/s)
1500	1.10
2500	1.45
3500	1.70
4500	2.00
5500	2.35

The values reported in Table 5 are used as the initial guess for velocity inlet boundary condition. Then, due to the influence of engine load on engine cooling, these values are modified so that the optimum coolant flow rate, which will be discussed in the following section, is derived.

According to Ref. [65] and the manufacturer, water jacket wall temperature at critical areas such as valve bridge is considered 413 K.

CHT method is used to predict the temperature of water jacket walls. This method simulates heat transfer between solid and fluid domains by exchanging thermal energy at the interfaces between them. Therefore, an interface that contains surfaces of solid parts and fluid parts should be defined due to different heat transfer equations for solid and fluid parts and also mesh changes because of material changes.

2.4. Boiling

In the engine water jacket, generally pure forced convection occurs, but in some critical regions such as the regions around the spark plug and exhaust valves, the temperature may exceed coolant saturation temperature. This circumstance leads to boiling. A MATLAB code is used to simulate the flow boiling phenomenon. The general equation for evaluating the subcooled flow boiling heat transfer is followed by equation (7) [66].

$$q'' = h_c\,(T_{wall} - T_c) + h_{nb}\,(T_{wall} - T_{sat}) \times S \tag{7}$$

where h_c is given by equation (8).

$$h_c = 0.023(k_c/D)Re^{0.8}\,Pr^{0.4} \tag{8}$$

In equations (7), (8)), h_{nb} is nucleate boiling convection coefficient, is coolant temperature, is the surface temperature of the heated wall, is saturation temperature, S is suppression factor and is coolant conductivity. The suppression factor, at first, was presented by Chen [67], but later, Steiner [68] presented a new and more precise suppression factor called S_{BDL}. Multiple correlations for predicting was proposed by some researchers. Qasemian and Keshavarz [66] showed that the combination of S_{BDL} and h_{nb} proposed by Gorenflo et al. [69] could estimate flow boiling heat transfer more accurately. Therefore, the heat transfer equation in the regions in which subcooled flow boiling occurs is as follows:

$$q'' = h_c\,(T_{wall} - T_c) + h_{nb,\,Gorenflo}\,(T_{wall} - T_{sat}) \times S_{BDL} \tag{9}$$

2.5. The appropriate value for the temperature of the engine water jacket

In today's ICEs, due to downsizing, the cooling system design should be based on using boiling phenomena in critical regions of the water jacket to enhance the cooling effect. The saturation temperature of the 50/50 water-EG at the pressure of 2 bar is 121 °C. Yu et al. [70] showed that the subcooled flow boiling in the ICE heat transfer condition generally occurs when the wall superheat is higher than 10°C. Furthermore, studying the subcooled flow boiling phenomena indicates that considering wall temperature up to 10 °C higher than the ONB is safe enough that it does not go over the critical heat flux (CHF). Therefore, the wall temperature of 140 °C can be considered as an appropriate wall temperature in critical temperature regions of the engine water jacket, as reported by Decan et al. [40]. As will be described in the rest of the paper, the smart cooling load-speed sensitive map is designed in a way that by changing the coolant mass flow rate, the temperature is kept at 140°C level.

3. Results and discussion

In this part, the results are given and discussed. As an important point, before any other explanations, it should be noted that the employed models have been validated for the investigated engine in the previous study of the research team [71] (as discussed completely in the introduction, the novelty of this paper is bringing a smart load-sensitive engine cooling map, and not presenting new models to simulate the engine performance). However, they are validated again in this part, as well. The details of validation are found in section 3.3. Before validation, the proposed smart engine cooling map is presented in section 3.1, and then, the enhancement potential of that is investigated in section 3.2.

3.1. The proposed smart engine cooling map

The proposed smart engine cooling map is presented here. Using the method whose flow chart is shown in Fig. 1, the profiles for the smart cooling map are determined. The process introduced in Fig. 1 is repeated for all the speeds and loads to obtain the engine cooling map. The values of flow rate are shown for the full load in Table 6. Water flow rates for 35°, 45°, and 67° open throttle angles are also given in Table 7a, Table 7b, and Table 7c, respectively.

Table 6. Flow rate and temperature at area between exhaust ports of 2nd cylinder head in WOT.

Engine RPM	$\dot{m}$(kg/s)	T_w (°C)(with boiling)	T_w (°C)(without boiling)
1500	1.20	140	175
2500	1.60	140	174
3500	1.85	140	174
4500	2.10	140	170
5500	2.60	140	171

Table 7a. Flow rate and temperature between exhaust ports of 2nd cylinder head at 35° open throttle angle.

Engine RPM	$\dot{m}$(kg/s)	T_w (°C)(with boiling)	T_w (°C)(without boiling)
1500	0.75	140	174
2500	1.05	140	172
3500	1.22	140	172
4500	1.40	140	171
5500	1.85	140	170

Table 7b. Flow rate and temperature between exhaust ports of 2nd cylinder head at 45° open throttle angle.

Engine RPM	ṁ(kg/s)	T_w (°C)(with boiling)	T_w (°C)(without boiling)
1500	0.90	140	174
2500	1.15	140	173
3500	1.30	140	173
4500	1.55	140	172
5500	2.00	140	170

Table 7c. Flow rate and temperature between exhaust ports of 2nd cylinder head at 67° open throttle angle.

Engine RPM	ṁ(kg/s)	T_w (°C)(with boiling)	T_w (°C)(without boiling)
1500	1.05	140	174
2500	1.25	140	174
3500	1.45	140	173
4500	1.75	140	172
5500	2.20	140	170

Fig. 11 shows the coolant flow rate depending on the engine speed and load, which is obtained from the proposed method indicated in Fig. 1. In fact, Fig. 11 depicts the smart speed-load sensitive engine cooling map.

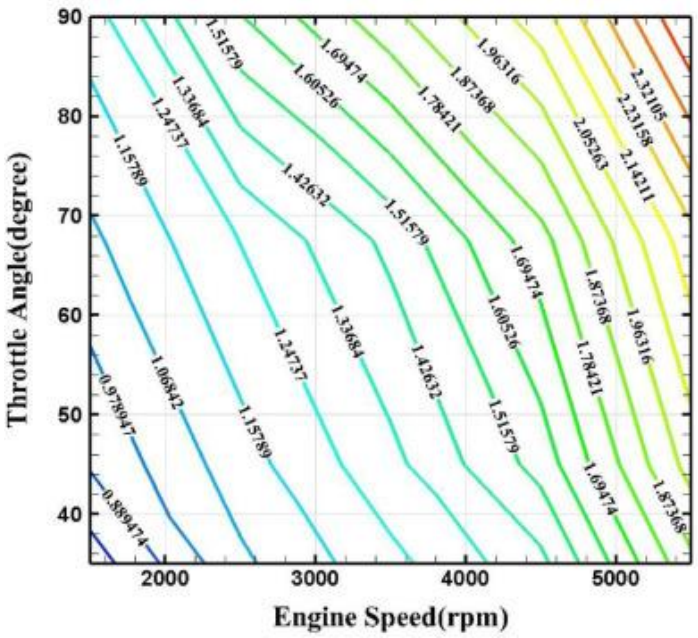

Fig. 11. Coolant flow rate (kg/s) map at different loads and speeds of the engine.

Fig. 11 shows that by the increase in speed and load, the coolant mass flow rate has an upward trend. In addition, at the higher speeds and load levels, the increase rate in the coolant mass flow rate is more than the lower values. The reason is by increasing engine load, the energy released in the engine increases because of increasing fuel flow rate. It raises heat dissipation by combustion process and temperature of engine parts, which means more coolant flow rate is needed. Moreover, when engine speed increases, number of cycles increases in a time unit. Like the increase in the engine load, increasing the speed leads to more heat release and higher temperature, which increases the required coolant flow rate. Between the speed and load (throttle angle), as Fig. 11 demonstrates, the impact of speed is more, but the effect of both of them is considerable.

Fig. 12 interprets the engine cooling map in a different way. In Fig. 12, variation of the coolant mass flow rate with engine speed in a constant throttle angle is presented.

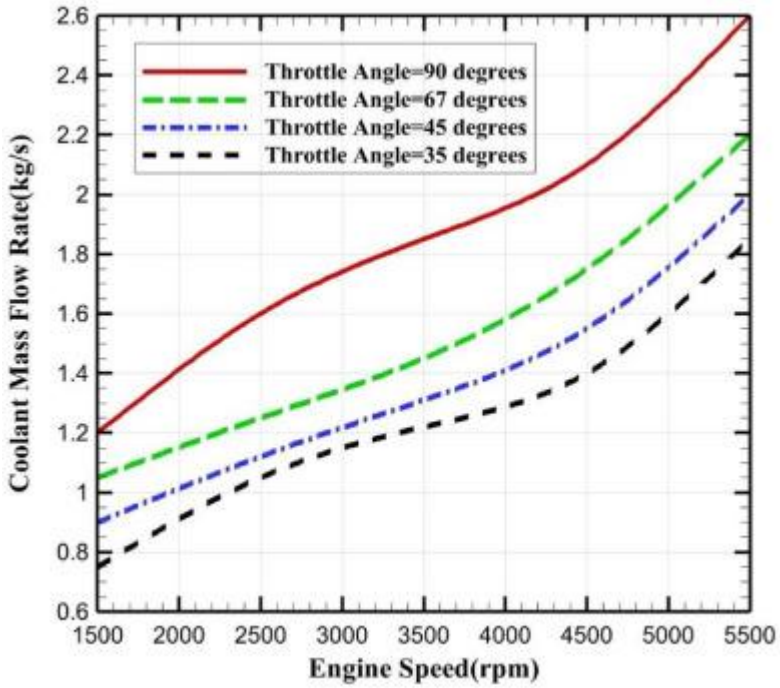

Fig. 12. Changes in the coolant flow rate by increase in engine speed.

The upward trend for coolant mass flow rate by increase in the engine speed at a constant load can be explained better with more details and quantitatively based on Fig. 12. For instance, in case the throttle angle of 67° is considered, changing the speed from 1500 to 3500 rpm is accompanied by 38% increase in the coolant mass flow rate while the corresponding value when the speed changes from 3500 to 5500 rpm is 51%. Fig. 13 provides the variation of coolant mass flow rate as a function of load for a number of engine speeds. Fig. 14 also represents a 3D picture of the engine cooling map.

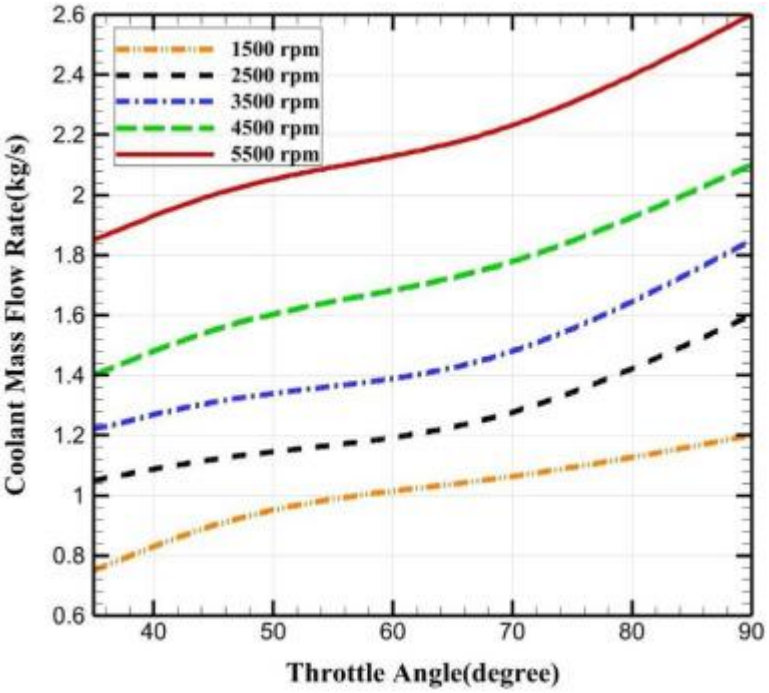

Fig. 13. Changes in the coolant flow rate by increase in throttle angle (load).

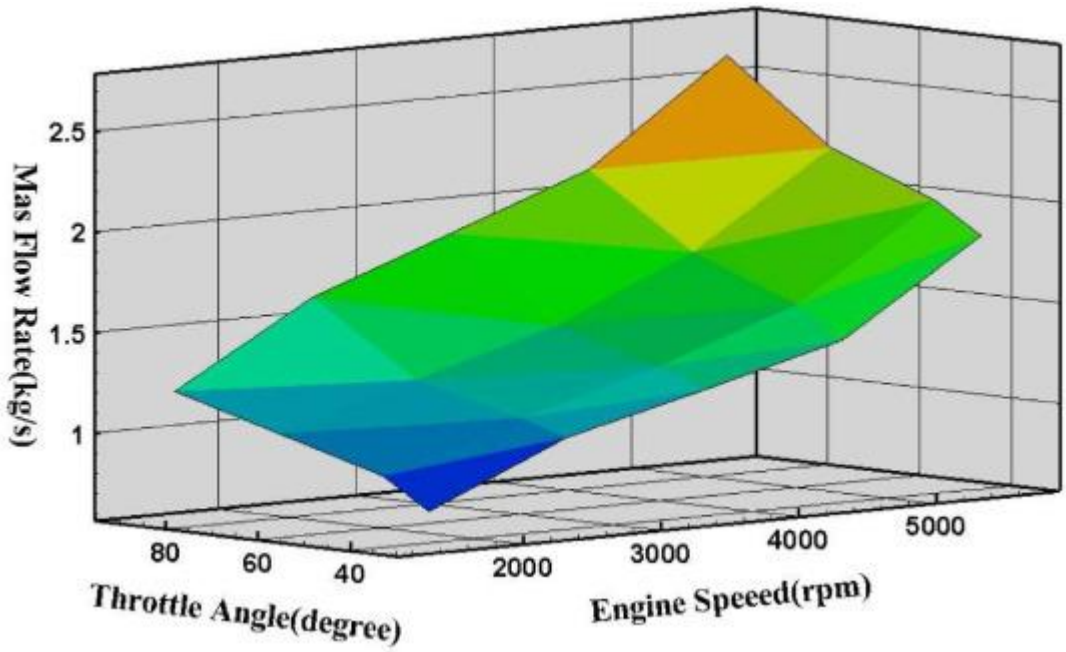

Fig. 14. The Contour map of coolant flow rate at different engine speeds and throttle angles.

The result shows that at a constant speed, increasing the load is accompanied by an almost linear increase in the coolant mass flow rate. However, the increase rate has an upward trend by an increase in the load, which leads to diverging the variation trend at high loads. Moreover, at a constant throttle angle, when speed goes up, the increase rate in the coolant mass flow rate increases as shown in Fig. 13. For instance, at the throttle angle of 67°, changing the speed from 2500 to 3500 rpm increases the coolant mass flow rate from 1.25 to 1.45 kg/s, which means 0.20 kg/s increase. When the speed goes 1000 rpm higher, and it reaches 4500 rpm, the mass

flow rate has 0.30 kg/s growth, and it is equal to 1.75 kg/s. The coolant mass flow rate for the speed of 5500 rpm is 2.20 kg/s, which shows it goes up 0.45 kg/s in comparison to 4500 rpm.

For further explanation, the values of reduction in pump power for different coolant flow rates due to applying coolant flow map at throttle position (THPS) of 45° are given in Table 8. Without a cooling flow map, the coolant flow rate is constant at any load and varies just in terms of engine speed. However, using a cooling flow map according to Fig. 12 or 13, the coolant flow rate changes at different loads, as well. As shown, applying smart cooling map leads to at least 35% reduction in pump power consumption. In addition, this coolant mass flow reduction decreases the size of the radiator and water pump.

Table 8. Effect of using cooling flow map on the water pump power reduction.

RPM	Conventional (constant at any load)				Smart cooling (@ THPS 45°)				Reduction of pump power (%)
	$\dot{m}_{conv}$ (kg/s)	ΔP_{eng} (Pa)	ΔP_{rad} (Pa)	$pump\ power_{conv}$ (W)	$\dot{m}_{new}$ (kg/s)	ΔP_{engine} (Pa)	ΔP_{rad} (Pa)	$pump\ power_{new}$ (W)	
1500	1.10	17,508	10,387	29.08	0.90	14,325	5930	17.28	40.59
2500	1.45	24,037	16,207	55.31	1.15	18,304	10653.7	31.56	42.93
3500	1.70	30,480	22,845	85.93	1.30	21,075	13,436	42.52	50.51
4500	2.00	42,000	30,024	136.54	1.55	26,012	18,786	65.82	51.80
5500	2.35	57,100	38,111	212.084	2.00	42,000	30,024	136.54	35.62

It is worth mentioning that for higher speeds, due to the higher coolant velocity, the convective heat transfer coefficient is higher, and the effect of boiling is reduced. Therefore, once again, it is proven that there is a need for a coolant flow rate map, similar to some other engine parameters such as spark.

3.2. Enhancement potential of applying the smart cooling map

In order to evaluate the enhancement potential of the proposed smart cooling map, the results of applying the map for two conditions from employing mechanical pump, which is shown in Fig. 15 and Fig. 16, are considered, and they are compared with the condition of employing the smart load-speed sensitive cooling map.

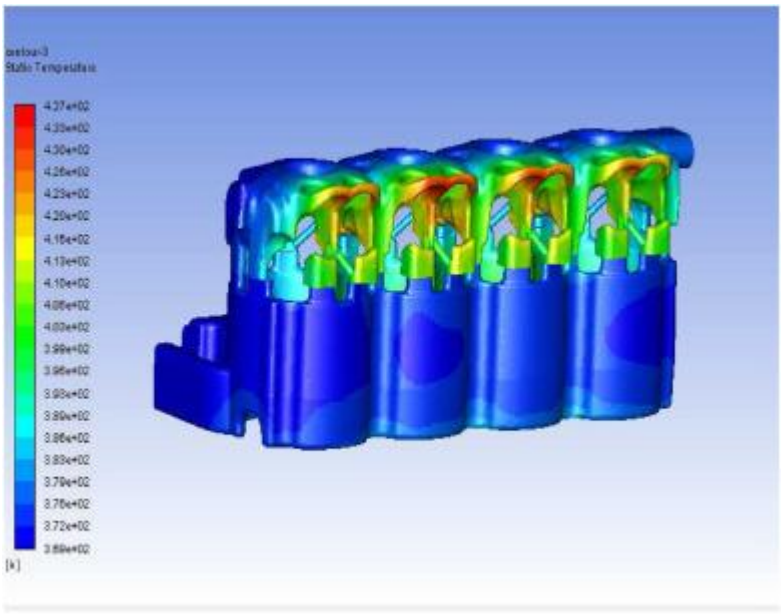

Fig. 15. Coolant temperature contour in 5500 rpm and 35° open throttle angle with 2.35 kg/s coolant flow rate (the conventional cooling system).

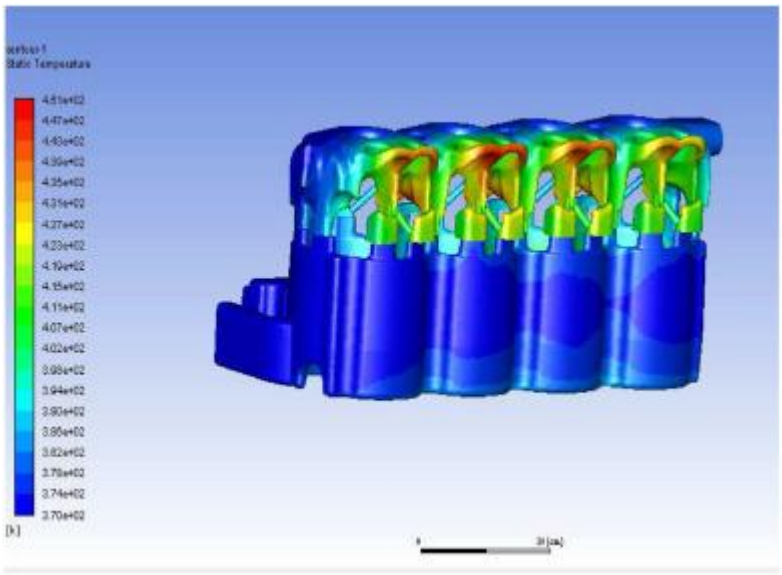

Fig. 16. Coolant temperature contour in 5500 rpm and WOT with 2.35 kg/s coolant flow rate (the conventional cooling system).

3.2.1. Employing the conventional cooling system

The boundary conditions at the combustion chamber and port walls are calculated in different values for the engine load and speed. Then, they are applied in the 3D simulation to obtain the thermal behavior of different parts of the engine, including water jackets. For both conditions, the conventional cooling system offers the coolant flow rate of 2.35 kg/s. For this coolant flow rate, i.e., the coolant flow rate of 2.35 kg/s, temperature contours of water jacket at 5500 rpm are illustrated at full throttle and 35°throttle angle in Figs. 15 and 16, respectively.

According to Figs. 15 and 16, it is observed that, the critical temperature region for water jacket of each cylinder is located between the exhaust ports. Moreover, the maximum temperature is observed in cylinder head No. 2. It happens because of the proximity of three sides of cylinder No. 1 with the air, while cylinder No. 2 is exposed to air in two sides. Another point is, at a fixed engine rpm, load considerably affects the temperature value, especially at the critical area.

Assuming a temperature of 140°C for water jacket wall temperature [40], Fig. 15 indicates that at 35° throttle angle (part-load) the maximum temperature without boiling assumption is 164°C, which is equal to 131 °C in consideration of the boiling. Therefore, over cooling occurs with flow rate of 2.35 kg/s. On the other hand, as shown in Fig. 16, the contours show that in the full load state, the maximum temperature reaches 178°C degrees regardless of boiling, which is equivalent to about 149°C, considering boiling. Consequently, the coolant flow rate of 2.35 kg/s is not able to meet the cooling requirements in some critical regions, and undercooling occurs by this flow rate. Therefore, the required flow rate should be more than 2.35 kg/s for the full load and less than 2.35 kg/s for part-load condition. It makes the shortcoming of the conventional cooling systems which only work based on the engine speed clear.

3.2.2. Employing the proposed smart load-speed sensitive cooling map

Fig. 17 and Fig. 18 are the temperature contours for the engine water jacket at 5500 rpm. In Fig. 17, the engine is run at full load and coolant flow rate of 2.60 kg/s, while in Fig. 18, the throttle angle is 35°, and coolant flow rate is 1.85 kg/s. Both coolant flow rates are obtained from the smart presented cooling map, i.e., Fig. 11.

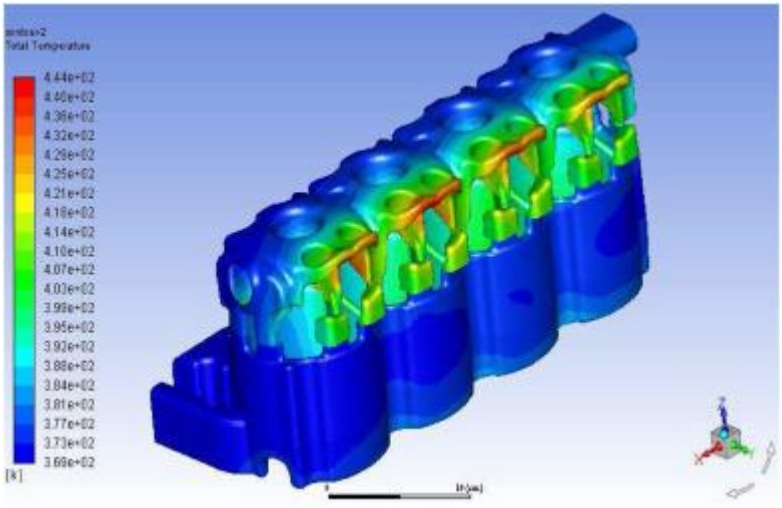

Fig. 17. Coolant temperature contour when the smart cooling map is applied in 5500 rpm and WOT flow rate of 2.60 kg/s (the smart load-speed sensitive cooling map).

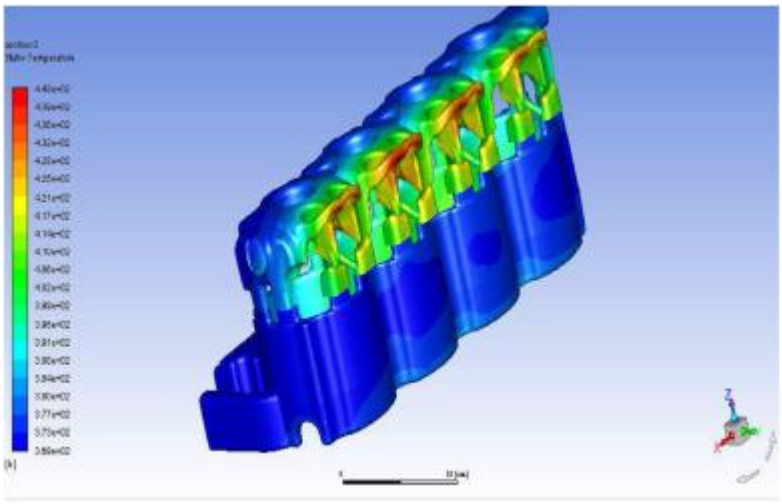

Fig. 18. Coolant temperature contour when the smart cooling map is applied in 5500 rpm and 35° open throttle angle in coolant flow rate is 1.85 kg/s (the smart load-speed sensitive cooling map).

As a result, it is found that compared to the coolant mass flow rate in the conventional engine cooling system for this speed, i.e., 2.35 kg/s, employing the smart load-sensitive performance map leads to 10.6 and 21.3% changes, respectively. It is a considerable change, and also diminishes the over and under cooling phenomena. As seen, the maximum temperature in both cases without boiling assumption is approximately 170°C, which is equal to 140°C when boiling effects are taken into account, and it leads to having a much greater engine performance. Moreover, based on the methodology presented in the references [22,33], the improvement in fuel consumption, hydrocarbon emission production, and needed power of the coolant pump has been computed for both conventional and smart cooling system, which shows that on average, they are enhanced by 2.1, 8.6, and 44.3%, respectively.

As the final point in this part, it should be noted that the analysis was conducted based on implementation of the electric water pump for the cooling circuit. The variable mass flow rate could be implemented using a valve (e.g., an electric servo valve) by which the water flow is controlled. A controlling system could be designed which has the developed smart-cooling map in its memory, and by giving feedback from the sensors to measure load and speed of the engine, the signal is sent to the valve to adjust the flow at the suggestion of the map. Considering the point that the main focus of this study was on finding the map, the comprehensive conceptual design of the controlling strategy is suggested as an idea for future works.

3.3. Validation

The details about validation of both 1D and 3D simulation approaches are described in this part. Validation is taken into account as a key element in each modeling approach to make sure that the model has enough accuracy [[72], [73], [74], [75]].

3.3.1. One dimensional simulation validation

Fig. 19 shows engine cylinder pressure at 5500 rpm and full load (WOT) experimentally and numerically. As shown in Fig. 19, there is good consistency between experimental and numerical results. In the methodology proposed in this study, the peak pressure and the gas temperature at the end of the power stroke should be carefully considered. The accuracy of the pressure

transducer applied in the combustion chamber is 1 kPa. The average error of numerical calculations and experimental data of the following diagram is 3.7%.

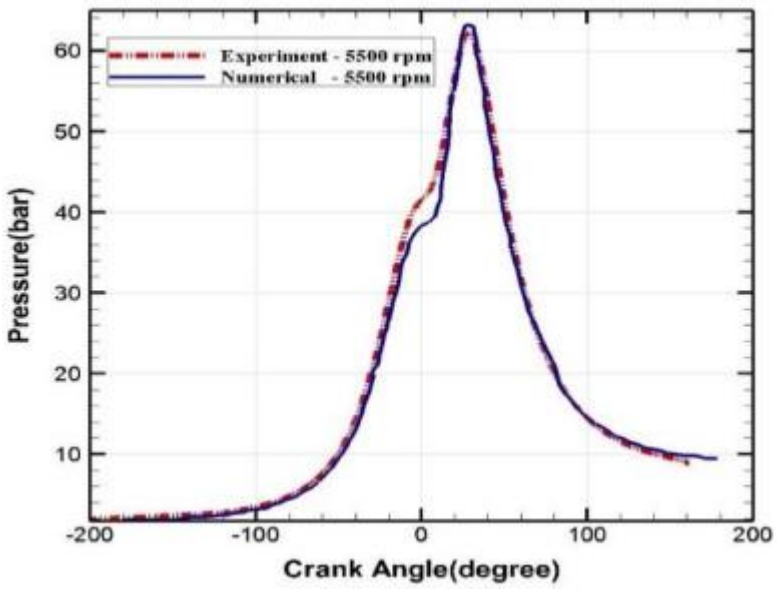

Fig. 19. Cylinder pressure at 5500 rpm and WOT.

Fig. 20 also compares the in-cylinder peak pressure obtained by experimental and numerical data at full load in terms of different engine speeds. As seen, the maximum error is related to 3000 rpm, which is around 5%. In this case, the average error is 2.66%.

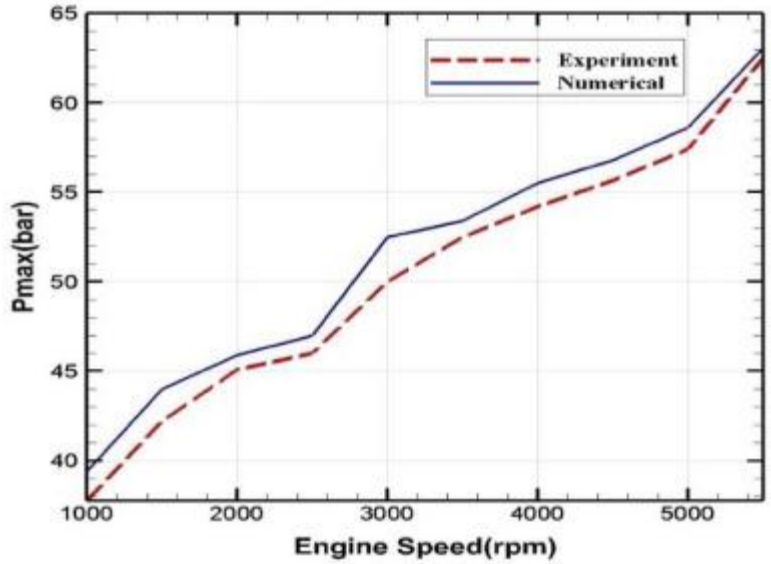

Fig. 20. The maximum cylinder pressure in different engine speeds and WOT.

Moreover, Fig. 21 compares the maximum cylinder pressure in experimental condition and numerical simulation in different engine speed and part load (BMEP = 8 bar). The maximum error occurs at 3500 rpm, which is 4.8%. Fig. 19, Fig. 20, Fig. 21 shows that good calculations have been made thermodynamically as a source of thermal boundary conditions.

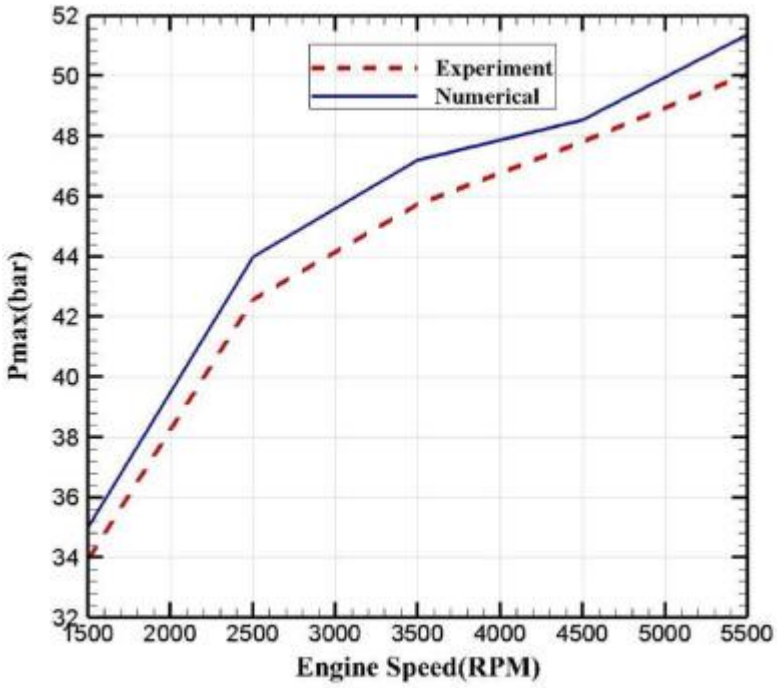

Fig. 21. The maximum cylinder pressure in the experimental condition and numerical simulation in different engine speeds and part loads (BMEP = 8 bar).

3.3.2. CFD simulation validation

3D simulation is validated by four parameters: mesh independency, Δp and ΔT of coolant along the coolant passage, and coolant velocity measurement by PIV method in two different coolant passage locations.

3.3.2.1. Pressure drop validation at coolant passage

Fig. 22 shows a schematic diagram of the experimental set up by which the coolant temperature and pressure difference along the engine coolant passage are measured.

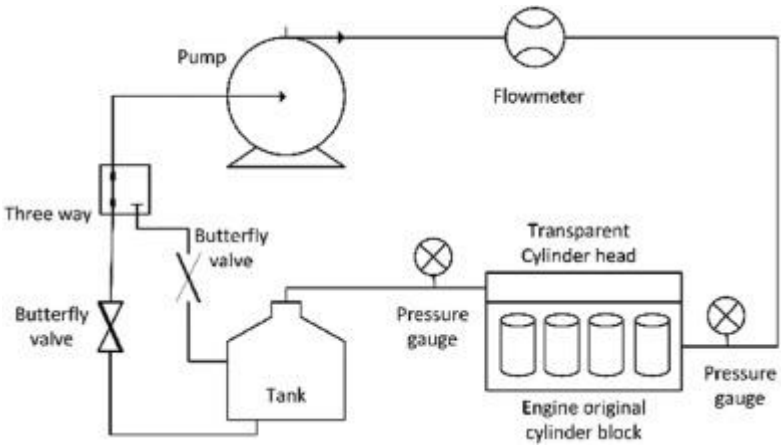

Fig. 22. Schematic layout of test bench for measuring the coolant temperature and pressure difference along the engine coolant passage [76].

The pressure drop and flow rate through the coolant passage is measured experimentally, as shown in Fig. 23. At water flow rate of 65 lit/min, pressure drop was measured as 9.8 kPa. The accuracy of pressure transmitter used for measuring the coolant pressure is ± 0.1 kPa. Numerical calculation of coolant passage pressure contours is shown in Fig. 24 and compared with experimental data in Table 9. As observed, there is a very good agreement between the model prediction and experiment.

(a)

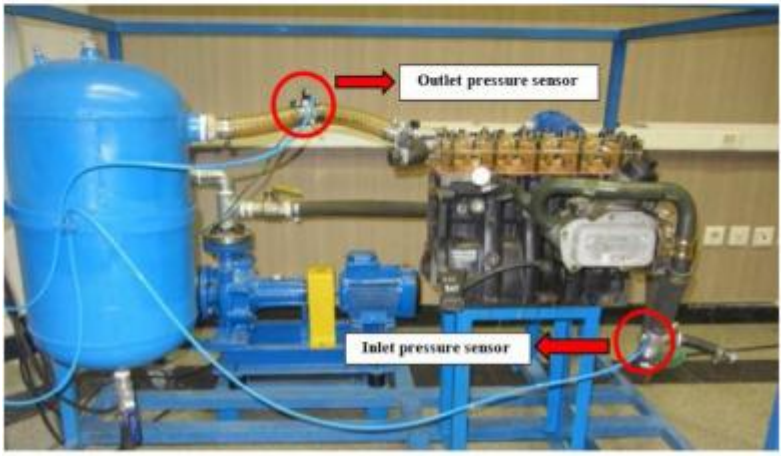

(b)

Fig. 23. Experimental case for pressure drop (a) Flow meter (b) Experimental setup.

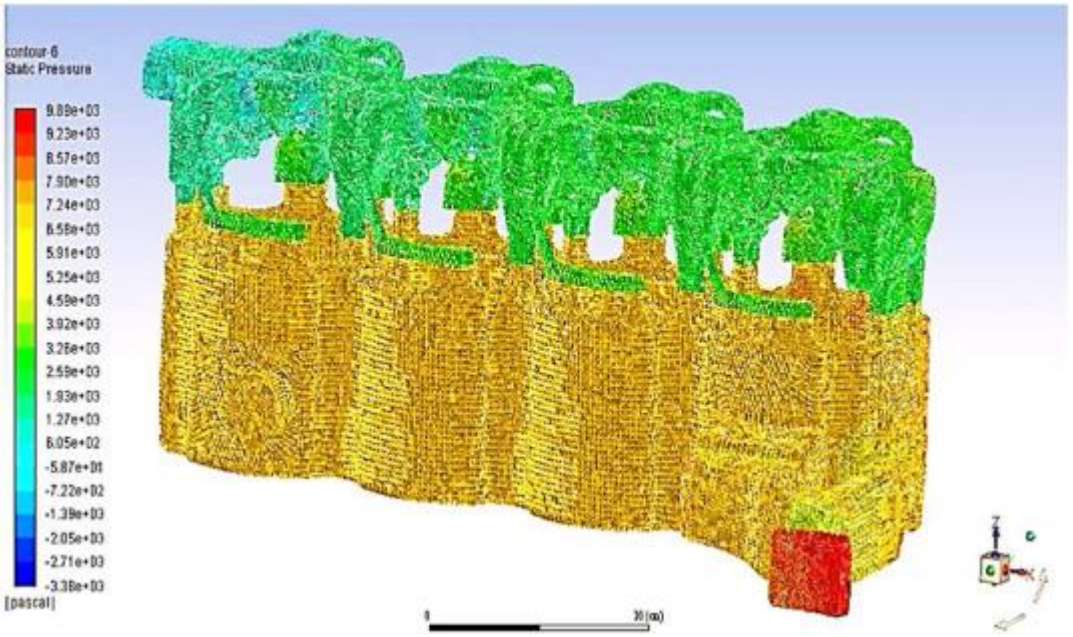

Fig. 24. Coolant pressure contour in 3000 rpm and WOT.

Table 9. Pressure drop at coolant passage.

data	Pressure drop (kPa)
Experimental	9.8
Simulation	9.811

3.3.2.2. Mesh independency

Table 10 shows pressure drop value for coolant flow rate of 65 lit/min with 4 different number of meshes. As seen in this table, for mesh numbers more than 2,832,881, despite considerable change of mesh number, pressure drop has no significant variation. Hence, this number of meshes is chosen for simulation.

Table 10. Pressure drop with different mesh numbers.

Mesh number	Pressure drop (kPa)
2,194,709	9.679
2,832,881	9.811
3,102,247	9.812
3,314,524	9.813

3.3.2.3. Temperature difference along the coolant passage

In both 3D simulation and experiment, the entrance coolant bulk temperature is 100°. Table 11 shows outlet coolant bulk temperature in 5500 rpm and WOT obtained by 3D simulation and experimental test. As presented in Table 11, the 3D simulation has good accuracy with the

experimental data. Temperature contour of coolant passage is represented in Fig. 25, as well. The accuracy of K type thermocouples used in this work is ±0.1°C.

Table 11. Coolant bulk temperature in passage.

FLUENT 3D simulation (°C)	Experimental data (°C)	Coolant bulk temperature
100	100	inlet
104	103.9	outlet

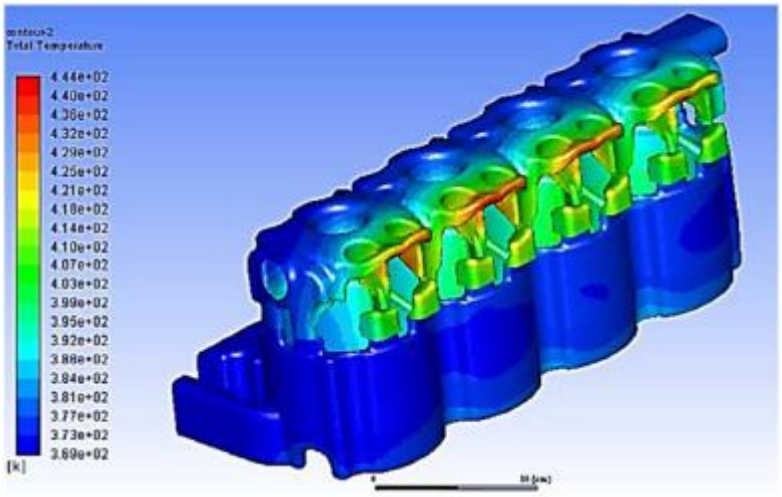

Fig. 25. Coolant temperature contour in 5500 rpm and WOT.

3.3.3. Validation of hydraulic simulation with PIV method

Particle Image Velocimetry (PIV) method was applied to validate CFD simulation. An experimental set up, shown in Fig. 26, was provided for this purpose. By passing the coolant flow through the transparent Plexiglas, shown in Fig. 27-a, coolant velocity at two different points (A) and (B) at 4th cylinder, as shown in Fig. 27-b, were measured experimentally.

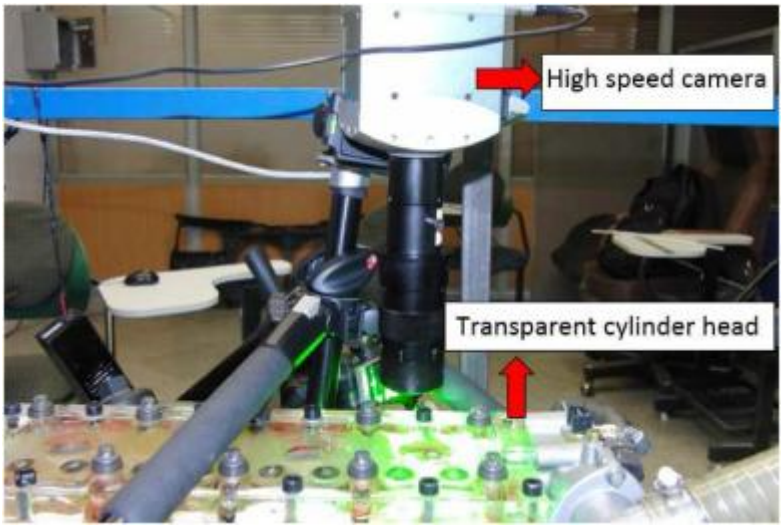

Fig. 26. Experimental setup to measure velocity [76].

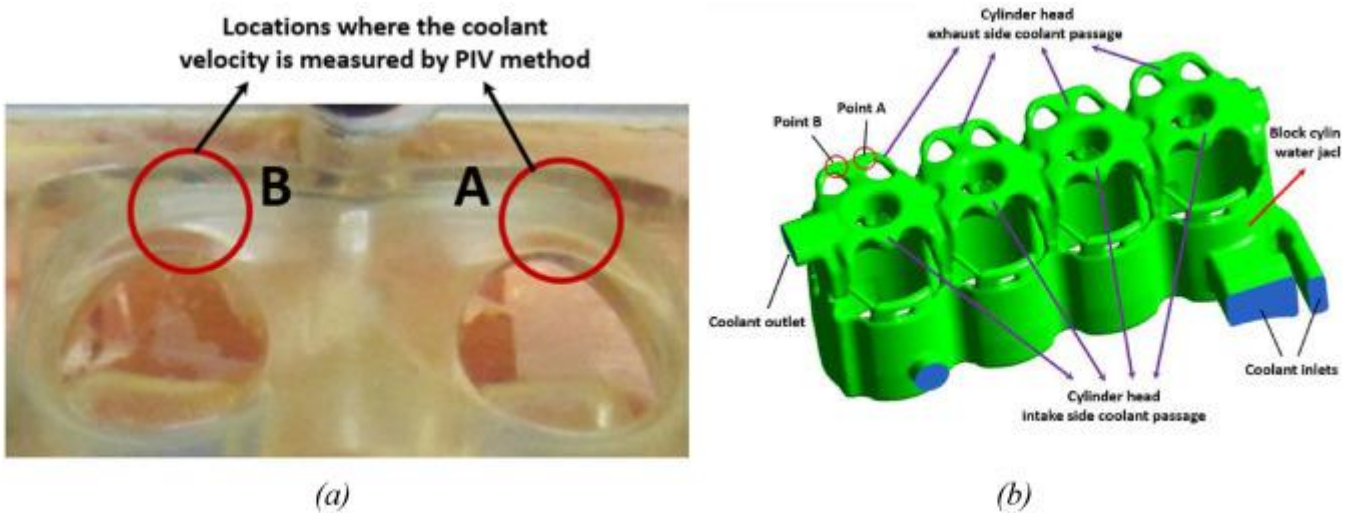

Fig. 27. Points A and B in 4th cylinder head. (a)Transparent cylinder head. (b) Coolant passage.

Velocity vectors obtained by CFD simulation and image processing of PIV method are demonstrated in Fig. 28-a and 28-b, respectively. Image processing of taken pictures, showed quantities of 0.7 m/s and 1.2 m/s for locations A and B, respectively [76].

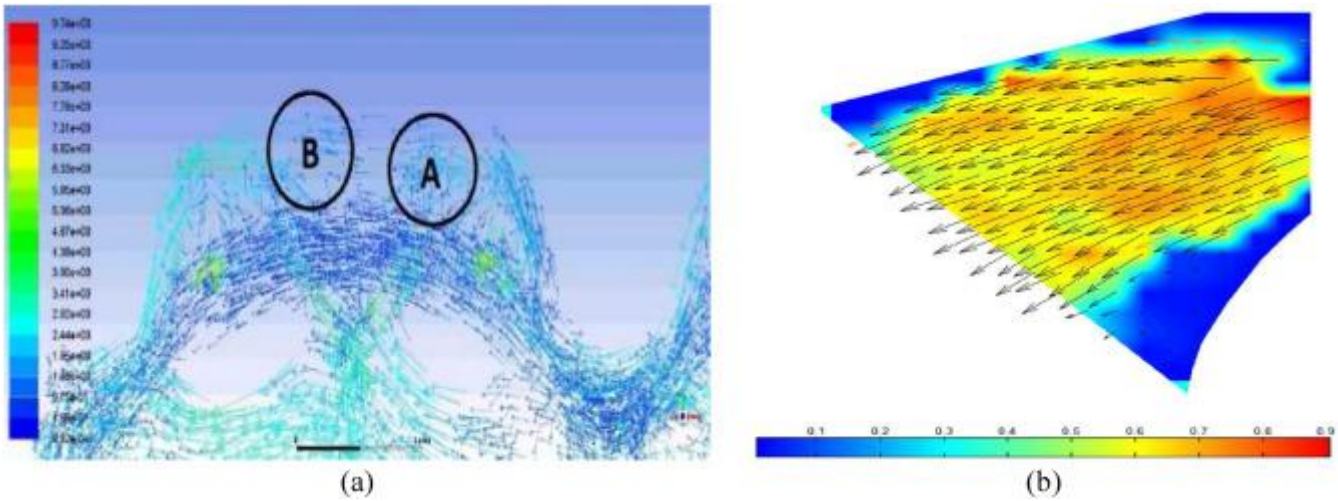

Fig. 28. Velocity vectors at measured point A by (a) CFD simulation (b) PIV method.

Velocity of mentioned points A and B, obtained by FLUENT 3D simulation and PIV method are given in Table 12. Comparison of the velocity values in these two locations, obtained by numerical and experimental methods, indicates good accuracy of CFD simulation.

Table 12. Coolant velocity in points A and B.

Point	Experimental data	FLUENT 3D simulation
	Velocity (m/s)	Velocity (m/s)
A	0.7	0.72
B	1.2	1.19

4. Conclusion

In order to enhance the performance of the cooling system in spark-ignition engines, a smart cooling map was proposed, based on the concept of using electric water pump. In this study, in addition to the speed, the engine load was taken into account for obtaining the smart cooling map. Finding the smart performance map of the cooling strategy was done by the numerical simulations, which worked based on 1D and 3D interactions, and in which the boiling effect is also considered.

A comprehensive comparative study between the conventional and proposed cooling strategies showed the huge benefits of the developed speed-load sensitive cooling map. It diminishes the significant difference among the maximum values for the temperature of the cylinder at different loads, which is a harmful phenomenon in the conventional cooling method. One of the most important advantages of using the load sensitive cooling map, along with reducing the coolant flow rate and consequently, water pump consumption and frictional mean effective pressure (FMEP), has been the optimal cooling management in order to eliminate overcooling and undercooling of the water jacket and creating a relatively uniform temperature distribution. On the other hand, by keeping the engine hot in such a way that the engine is kept free from damage, the efficiency of the internal combustion engine as a heat engine according to the ideal Carnot cycle increases. In addition, a relatively uniform temperature in the engine body is obtained due to reducing cylinder to cylinder variation as an undesirable phenomenon in the engine.

Declaration of competing interest

The authors declare that they have no known competing financial interests or personal relationships that could have appeared to influence the work reported in this paper.

Acknowledgments

This research project was partially supported by Irankhodro Powertrain Company (IPCo). We all thank Mr. Rajabali, who generously provided his insight and expertise to this study.

References

[1] Djouadi A, Bentahar F. Combustion study of a spark-ignition engine from pressure cycles. Energy 2016; 101:211e7.
[2] Loaiza Bernal JL, Ferreira JV. Model of water injection process during closed phase of spark ignition engine. Energy 2019; 174:1121e32.
[3] Porpatham E, Ramesh A, Nagalingam B. Experimental studies on the effects of enhancing the concentration of oxygen in the inducted charge of a biogas fuelled spark ignition engine. Energy 2018; 142:303e12.
[4] Sohani A, Rezapour S, Sayyaadi H. Comprehensive performance evaluation and demands' sensitivity analysis of different optimum sizing strategies for a combined cooling, heating, and power system. J Clean Prod 2021; 279:123225.
[5] Akkoli KM, Banapurmath NR, Shivashimpi MM, Soudagar MEM, Badruddin IA, Alazwari MA, Yaliwal VS, Mujtaba MA, Akram N, Goodarzi M, Safaei MR, Venu H. Effect of injection parameters and producer gas derived from redgram stalk on the performance and emission characteristics of a diesel engine. Alexandria Eng J 2021;60(3):3133e42.
[6] Campo A, Ar1C1 M. Semi-analytical solution of the graetz problem with uniform wall heat flux utilizing the transversal method of lines. J Heat Tran 2020;142(4).

[7] Soudagar MEM, Afzal A, Safaei MR, Manokar AM, El-Seesy AI, Mujtaba MA, Samuel OD, Badruddin IA, Ahmed W, Shahapurkar K. Investigation on the effect of cottonseed oil blended with different percentages of octanol and suspended MWCNT nanoparticles on diesel engine characteristics. J Therm Anal Calorim 2020:1e18.
[8] Doranehgard MH, Samadyar H, Mesbah M, Haratipour P, Samiezade S. Highpurity hydrogen production with in situ CO2 capture based on biomass gasification. Fuel 2017; 202:29e35.
[9] Tornatore C, Bozza F, De Bellis V, Teodosio L, Valentino G, Marchitto L. Experimental and numerical study on the influence of cooled EGR on knock tendency, performance and emissions of a downsized spark-ignition engine. Energy 2019; 172:968e76.
[10] Soudagar MEM, Mujtaba MA, Safaei MR, Afzal A, V DR, Ahmed W, Banapurmath NR, Hossain N, Bashir S, Badruddin IA, Goodarzi M, Shahapurkar K, Taqui SN. Effect of Sr@ZnO nanoparticles and Ricinus communis biodiesel-diesel fuel blends on modified CRDI diesel engine characteristics. Energy 2021; 215:119094.
[11] Sandro N, Agis P, Gojmir R, Vlasta Z, Müslüm A. Using pellet fuels for residential heating: a field study on its efficiency and the users' satisfaction. Energy Build 2019; 184:193e204.
[12] Elfasakhany A. Exhaust emissions and performance of ternary iso-butanolebio-methanolegasoline and n-butanolebio-ethanolegasoline fuel blends in spark-ignition engines: assessment and comparison. Energy 2018;158: 830e44.
[13] Duan X, Liu J, Yao J, Chen Z, Wu C, Chen C, Dong H. Performance, combustion and knock assessment of a high compression ratio and lean-burn heavy-duty spark-ignition engine fuelled with n-butane and liquefied methane gas blend. Energy 2018; 158:256e68.
[14] Khan H, Soudagar MEM, Kumar RH, Safaei MR, Farooq M, Khidmatgar A, Banapurmath NR, Farade RA, Abbas MM, Afzal A. Effect of nano-graphene oxide and n-butanol fuel additives blended with dieseldnigella sativa biodiesel fuel emulsion on diesel engine characteristics. Symmetry 2020;12(6): 961.
[15] Ashour MK, Eldrainy YA, Elwardany AE. Effect of cracked naphtha/biodiesel/ diesel blends on performance, combustion and emissions characteristics of compression ignition engine. Energy 2020; 192:116590.
[16] Mahdisoozani H, Mohsenizadeh M, Bahiraei M, Kasaeian A, Daneshvar A, Goodarzi M, Safaei MR. Performance enhancement of internal combustion engines through vibration control: state of the art and challenges. Appl Sci 2019;9(3):406.
[17] Thakur AK, Prabakaran R, Elkadeem MR, Sharshir SW, Ar1c1 M, Wang C, Zhao W, Hwang J-Y, Saidur R. A state of art review and future viewpoint on advance cooling techniques for Lithiumeion battery system of electric vehicles. J Energy Storage 2020; 32:101771.
[18] Sohani A, Naderi S, Torabi F. Comprehensive comparative evaluation of different possible optimization scenarios for a polymer electrolyte membrane fuel cell. Energy Convers Manag 2019; 191:247e60.
[19] Chen Z, Ai Y, Qin T, Luo F. Quantitative evaluation of n-butane concentration on knock severity of a natural gas heavy-duty SI engine. Energy 2019;189: 116244.
[20] Serrano J, Jimenez-Espadafor FJ, L opez A. Analysis of the effect of different hydrogen/diesel ratios on the performance and emissions of a modified compression ignition engine under dual-fuel mode with water injection. Hydrogen-diesel dual-fuel mode. Energy 2019; 172:702e11.
[21] Sadeghinezhad E, Kazi SN, Sadeghinejad F, Badarudin A, Mehrali M, Sadri R, Reza Safaei M. A comprehensive literature review of bio-fuel performance in internal combustion engine and relevant costs involvement. Renew Sustain Energy Rev 2014; 30:29e44.
[22] Samiezadeh S, Qasemian A, Sohani A, Rezaei A, Khodaverdian R, Soltani R, et al. Energy and environmental enhancement of power generation units by means of zero-flow coolant strategy. Int J Energy Res 2021. https://doi.org/ 10.1002/er.6498.

[23] Burke RD, Lewis AJ, Akehurst S, Brace CJ, Pegg I, Stark R. Systems optimisation of an active thermal management system during engine warm-up. Part D: J Automobile Eng 2012;226(10):1365e79.
[24] Cho H, Jung D, Filipi ZS, Assanis DN, Vanderslice J, Bryzik W. Application of controllable electric coolant pump for fuel economy and cooling performance improvement. 2007.
[25] Choi K-W, Kim K-B, Lee K-H. Technology, Investigation of emission characteristics affected by new cooling system in a diesel engine. J Mech Sci Technol 2009;23(7):1866e70.
[26] Jeong S-J, Kim W-s, Oh C-B, Park J-k, Lee H-k, Oh S-d, Chun H-h. An experimental study on the clutch-type water pump of diesel passenger vehicle for reducing fuel consumption and CO2 emission. In: ASME-JSME-KSME 2011 joint fluids engineering conference. American Society of Mechanical Engineers Digital Collection; 2011. p. 893e903.
[27] Wang TT, Wagner JR. A smart engine cooling system-experimental study of integrated actuator transient behavior. SAE Technical Paper; 2015.
[28] Wagner JR, Srinivasan V, Dawson DM, Marotta EE. Smart thermostat and coolant pump control for engine thermal management systems. SAE Technical Paper; 2003.
[29] Negandhi V, Jung D, Shutty J. Active Thermal management with a dual mode coolant pump. 2013-01-0849 SAE Int J Passenger Cars-Mech Syst 2013;6: 817e25.
[30] Cai W, Xiong S, Fang L, Zha S. Electric water-pump development for cooling gasoline engine. In: Proceedings of the FISITA 2012 world automotive congress. Springer; 2013. p. 1345e56.
[31] Chastain J, Wagner J, Eberth JJIPV. Advanced engine coolingecomponents. Testing Observ. 2010;43(7):294e9.
[32] Shin YH, Kim SC, Kim MSJE. Use of electromagnetic clutch water pumps in vehicle engine cooling systems to reduce fuel consumption 2013; 57:624e31.
[33] Mohamed ES. Development and analysis of a variable position thermostat for smart cooling system of a light duty diesel vehicles and engine emissions assessment during NEDC. Appl Therm Eng 2016; 99:358e72.
[34] Mohamed ES, Allam EM. Technology, Effect of active cooling control on internal combustion engine exhaust emissions and instantaneous performance enhancement. Curr J Appl Sci Technol 2016:1e16.
[35] Haghighat AK, Roumi S, Madani N, Bahmanpour D, Olsen MG. An intelligent cooling system and control model for improved engine thermal management. Appl Therm Eng 2018; 128:253e63.
[36] Castiglione T, Pizzonia F, Piccione R, Bova S. Detecting the onset of nucleate boiling in internal combustion engines. Appl Energy 2016; 164:332e40.
[37] Annabattula P, Iqbal O, Sanka M, Arora K. Sizing of coolant passages in an IC engine Using a Design of Experiments Approach. SAE Int J Eng 2015;8(4): 1898e905.
[38] Hassan MI, Brimmo AT. Modeling in-cylinder water injection in a 2-stroke internal combustion engine. Energy Procedia 2015; 75:2331e6.
[39] Ali MH, Hassan M, Kalam M, Pang SC, Memon L, Magami I. Determination of time variant 1d-3d temperature and heat transfer distribution inside the cooling jacket of a si engine cooling system after key-off. In: SAE technical paper; 2012.
[40] Decan G, Broekaert S, Lucchini T, D'Errico G, Vierendeels J, Verhelst S. Evaluation of wall heat flux models for full cycle CFD simulation of internal combustion engines under motoring operation. In: SAE technical paper; 2017.
[41] Decan G, Broekaert S, Lucchini T, D'Errico G, Vierendeels J, Verhelst S. Evaluation of wall heat flux calculation methods for CFD simulations of an internal combustion engine under both motored and HCCI operation. Appl Energy 2018; 232:451e61.
[42] Schmitt M, Frouzakis CE, Wright YM, Tomboulides AG, Boulouchos K. Direct numerical simulation of the compression stroke under engine-relevant conditions: evolution of the velocity and thermal boundary layers. Int J Heat Mass Tran 2015; 91:948e60.

[43] Mauro S, S¸ener R, Gül M, Lanzafame R, Messina M, Brusca S. Internal combustion engine heat release calculation using single-zone and CFD 3D numerical models. Int J Energy Environ Eng 2018;9(2):215e26.
[44] Jo YS, Lewis R, Bromberg L, Heywood JB. Performance maps of turbocharged SI engines with gasoline-ethanol blends: torque, efficiency, compression ratio, knock limits, and octane. In: SAE technical paper; 2014.
[45] Wu M, Pei Y, Qin J, Li X, Zhou J, Zhan ZS, Guo Q-y, Liu B, Hu TG. Study on methods of coupling numerical simulation of conjugate heat transfer and incylinder combustion process in GDI engine. In: SAE technical paper; 2017.
[46] Saric S, Basara B, Zunic Z, Flow F. Advanced near-wall modeling for engine heat transfer. Int J Heat Fluid Flow 2017; 63:205e11.
[47] Berni F, Cicalese G, Fontanesi SJATE. A modified thermal wall function for the estimation of gas-to-wall heat fluxes in CFD in-cylinder simulations of high performance spark-ignition engines 2017; 115:1045e62.
[48] Han Z, Reitz RD, transfer m. A temperature wall function formulation for variable-density turbulent flows with application to engine convective heat transfer modeling. Int J Heat Mass Transfer 1997;40(3):613e25.
[49] Angelberger C, Poinsot T, Delhay B. Improving near-wall combustion and wall heat transfer modeling in SI engine computations. In: SAE technical paper; 1997.
[50] Cicalese G, Berni F, Fontanesi S, d'Adamo A, Andreoli E. A comprehensive CFDcht methodology for the characterization of a diesel engine: from the heat transfer prediction to the thermal field evaluation. In: SAE technical paper; 2017.
[51] Broatch A, Olmeda P, Margot X, Escalona J. New approach to study the heat transfer in internal combustion engines by 3D modelling. Int J Therm Sci 2019; 138:405e15.
[52] Harada Y, Uchida K, Tanaka T, Sato K, Zhu Q, Fujimoto H, Yamashita H, Tanahashi M. Wall heat transfer of unsteady near-wall flow in internal combustion engines. Int J Engine Res 2019; vol. 20:817e33.
[53] Ma PC, Greene M, Sick V, Ihme M. Non-equilibrium wall-modeling for internal combustion engine simulations with wall heat transfer. Int J Engine Res 2017;18(1e2):15e25.
[54] Li Y, Kong S-C. Coupling conjugate heat transfer with in-cylinder combustion modeling for engine simulation. Int J Heat Mass Tran 2011;54(11):2467e78.
[55] Zhang L. Parallel simulation of engine in-cylinder processes with conjugate heat transfer modeling. Appl Therm Eng 2018; 142:232e40.
[56] Keum S, Park H, Babajimopoulos A, Assanis D, Jung D. Modelling of heat transfer in internal combustion engines with variable density effect. Int J Engine Res 2011;12(6):513e26.
[57] Ferguson CR, Kirkpatrick AT. Internal combustion engines: applied thermosciences. John Wiley & Sons; 2015.
[58] Andruskiewicz P, Najt P, Durrett R, Biesboer S, Schaedler T, Payri R. Analysis of the effects of wall temperature swing on reciprocating internal combustion engine processes. Int J Eng Res 2018;19(4):461e73.
[59] Winkler N. Effect of pressure oscillations on in-cylinder heat transferethrough large eddy simulation. Int J Eng Research 2015;16(6): 705e15.
[60] Heywood BJ. Internal combustion engine fundamentals. 1988.
[61] Fluent A. 19.2 theory guide. ANSYS; 2018 [in, Inc].
[62] Bergman TL, Incropera FP, DeWitt DP, Lavine AS. Fundamentals of heat and mass transfer. John Wiley & Sons; 2011.
[63] Depcik C, Assanis DJST. A universal heat transfer correlation for intake and exhaust flows in an spark-ignition internal combustion engine. 2002. p. 734e40.
[64] Kumar V, Kapoor S, Arora G, Saha SK, Dutta P. A combined CFD and flow network modeling approach for vehicle underhood air flow and thermal analysis. SAE Technical Paper; 2009.

[65] Clough MJST. Precision cooling of a four valve per cylinder engine. 1993. p. 1555e66.
[66] Qasemian A, Keshavarz A. Robust empirical correlation development for subcooled flow boiling heat transfer in internal combustion engines. Int J Sci Eng Res 2015;5(11).
[67] Chen JCJI, e.c.p. design, development. Correlation for boiling heat transfer to saturated fluids in convective flow 1966;5(3):322e9.
[68] Steiner H, Kobor A, Gebhard L. A wall heat transfer model for subcooled boiling flow. Int J Heat Mass Tran 2005;48(19):4161e73.
[69] Gorenflo D, Chandra U, Kotthoff S, Luke A. Influence of thermophysical properties on pool boiling heat transfer of refrigerants. Int J Refrig 2004;27(5): 492e502.
[70] Yu W, France DM, Singh D, Smith RK, Ritter J, Vijlbrief T, Menger Y. Subcooled flow boiling of ethylene glycol/water mixtures in a bottom-heated tube. Int J Heat Mass Tran 2014; 72:637e45.
[71] Qasemian A, Keshavarz A. Experimental and numerical study of an internal combustion engine coolant flow distribution/Eksperimentalna i numericka analiza raspodjele toka rashladnog sredstva u motoru s unutarnjim izgaranjem. Tehnicki Vjesnik-Techn Gazette 2016;23(1):257e65.
[72] Yıldız Ç, Arıcı M, Nizetic S, Shahsavar A. Numerical investigation of natural convection behavior of molten PCM in an enclosure having rectangular and tree-like branching fins. Energy 2020; 207: 118223.
[73] Sohani A, Hoseinzadeh S, Berenjkar K. Experimental analysis of innovative designs for solar still desalination technologies; an in-depth technical and economic assessment. J Energy Storage 2021; 33:101862.
[74] Sohani A, Shahverdian MH, Sayyaadi H, Garcia DA. Impact of absolute and relative humidity on the performance of mono and poly crystalline silicon photovoltaics; applying artificial neural network. J Clean Prod 2020;276: 123016.
[75] Sohani A, Sayyaadi H. Employing genetic programming to find the best correlation to predict temperature of solar photovoltaic panels. Energy Convers Manag 2020; 224:113291.
[76] Qasemian AKA. Eksperimentalna i numeri_cka analiza raspodjele toka rashladnog sredstva u motoru s unutarnjim izgaranjem. Teh Vjesn 2016;23: 257e64. br. 1, str.